Catalysis Science & Technology

ROYAL SOCIETY OF CHEMISTRY

PAPER

View Article Online
View Journal | View Issue

Check for updates

Cite this: *Catal. Sci. Technol.*, 2023, 13, 6006

Understanding structure–activity relationships: iron(II) complexes of "Legacy Guanidines" as catalysts for the synthesis of polylactide†

Christian Conrads, Lisa Burkart, Sven Soerensen, Sandra Noichl, Yasemin Kara, Joshua Heck, Alexander Hoffmann and Sonja Herres-Pawlis *

Received 11th August 2023,
Accepted 17th September 2023

DOI: 10.1039/d3cy01117h

rsc.li/catalysis

In this work, eight novel iron(II) chloride complexes of well-known bisguanidine and N,N hybrid guanidine ligands are presented. Their activity in the synthesis of polylactide *via* a ring-opening polymerization was investigated under industrially relevant conditions with low catalyst loadings in the lactide melt. The conversion was monitored by *in situ* Raman spectroscopy to evaluate the reaction kinetics. The catalysts were investigated regarding their polymerization activity as well as their ability to maintain their polymerization activity over time. The most promising catalyst [Fe(TMGepy)Cl_2] (**C6**) polymerizes L-lactide at monomer-to-initiator ratios of 1000 : 1 and higher with a rate constant of propagation similar to the until now most active robust iron catalysts. Experiments on the influence of a co-initiator were carried out. Additionally, the experimental observations were further underlined with theoretical calculations explaining the stability and activity of the catalysts. Iron guanidines with rather simple ligands demonstrate a great potential for large-scale application in the industrial process. Finally, initial tests on the application of the compounds in the methanolysis of polylactide were conducted.

Introduction

Polylactic acid or polylactide (PLA) has been the focus of many research groups in the last two decades because it is bio-based as well as biodegradable and features properties resembling conventional plastics.[1–3] Moreover, it serves as an excellent example of a plastic with a large potential for the circular economy offering various options for recycling, including mechanical and chemical recycling.[4,5] The preparation of PLA *via* the ring-opening polymerization (ROP) of lactide is well-established and has been discussed in numerous publications following anionic,[6] cationic,[7] organocatalytic[8] and coordination–insertion[9] mechanisms. The latter takes a special role because it exhibits a high tolerance towards impurities and allows a controlled polymerization behavior. Complexes of various transition and main group metals were successfully applied as catalysts including complexes of Mg,[10] Al,[11] Fe,[12–18] Zn,[19–21] Zr,[22] La[23,24] and many more.

However, only a rather small number of publications focused on catalysts that are appropriate for the industrially-relevant melt polymerization of lactide. Besides a sufficient activity, this requires an inexpensive and straightforward preparation of the metal complex, a sufficient stability towards impurities and temperature as well as control over the molar mass and dispersity.[25] Additionally, the use of non-toxic metal catalysts is desirable instead of the commonly used tin(II) octoate ($Sn(Oct)_2$).[26] Numerous examples of robust guanidine catalysts based on bio-compatible iron or zinc metal ions were published by our group.[27–30] Guanidines are strong organic bases and excellent neutral N donor ligands coordinating *via* the imine nitrogen atom. The most common guanidine units are the peralkylated tetramethylguanidine (TMG) and dimethylethyleneguanidine (DMEG) units (see Fig. 1A). The library of already published guanidine containing ligands is versatile.[31,32] The ligands vary in the number of guanidine units, additional donor units (*e.g.* pyridines, quinolines, esters), the distance between donor units and the type of the ligand backbone which can be either aromatic or aliphatic (see Fig. 1B and C).

The interest in multidentate guanidine ligands dates back to the year 2000, when the first examples of bisguanidine ligands such as propylene-bridged TMG_2p (**L4**, also known as btmgp)[33–35] and the ethylene-bridged TMG_2e (**L3**)[35] were presented. In the field of lactide polymerization first attempts were made with zinc complexes of bisguanidine and N,N

Institute of Inorganic Chemistry, RWTH Aachen University, Landoltweg 1a, 52074 Aachen, Germany. E-mail: sonja.herres-pawlis@ac.rwth-aachen.de

† Electronic supplementary information (ESI) available: Details of analytical methods, crystallographic information, TGA results, experimental data for polymerization and depolymerization, DSC results, MALDI-TOF-MS results, DFT details. CCDC 2278551–2278549. For ESI and crystallographic data in CIF or other electronic format see DOI: https://doi.org/10.1039/d3cy01117h

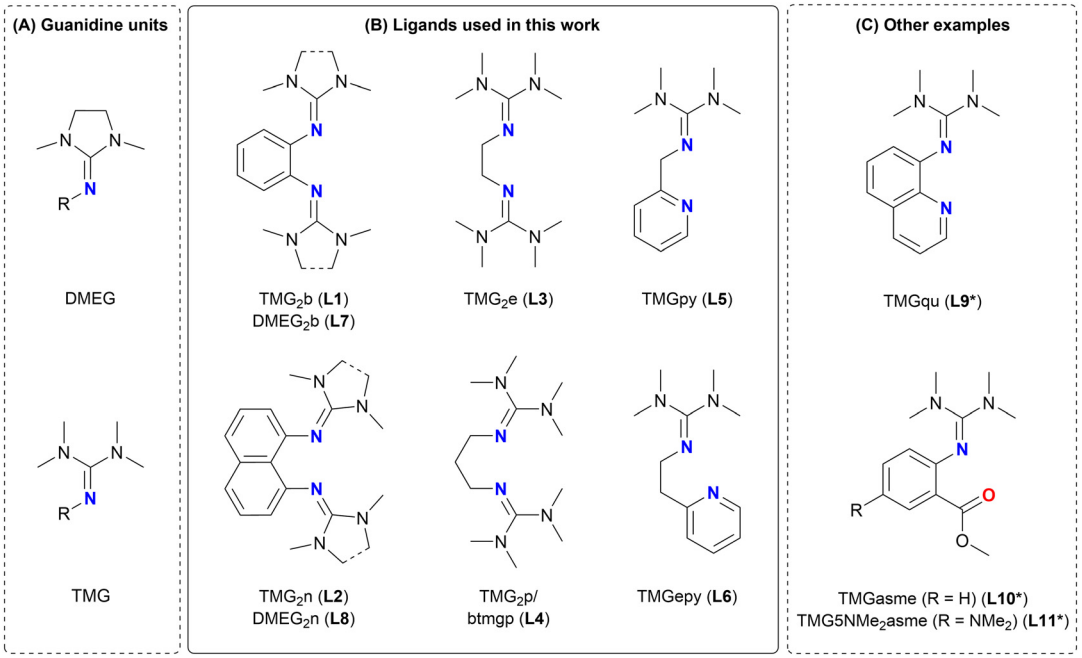

Fig. 1 (A) Structures of the DMEG and TMG units. (B) Structures of literature-known bisguanidine and N,N hybrid guanidine ligands used in this work: **L1**: TMG_2b;[45] **L2**: TMG_2n;[46] **L3**: TMG_2e;[35] **L4**: TMG_2p/btmgp;[33,35] **L5**: TMGpy;[49] **L6**: TMGepy;[50] **L7**: $DMEG_2b$;[47] **L8**: $DMEG_2n$.[48] (C) Other examples of N,N and N,O hybrid guanidine ligands: **L9***: TMGqu;[49] **L10***: TMGasme;[38] **L11***: $TMG5NMe_2asme$.[39,40]

hybrid guanidine ligands such as $DMEG_2e$,[36] the guanidine–pyridine hybrid ligands TMGpy (**L5**)/DMEGpy[37] and the guanidine–quinoline hybrid ligands TMGqu (**L9***)/DMEGqu.[37] These complexes proved to be active in the bulk polymerization of lactide, however, on a rather large time scale of several hours to days exhibiting a significantly lower activity than the industrially-applied tin(II) octoate. A major step towards catching up tin(II) octoate was made when the first zinc chloride and zinc bromide complexes with N,O hybrid guanidine ligands (TMGasme (**L10***)/DMEGasme, see Fig. 1C) were introduced to the lactide polymerization.[38] The ligand system was later further optimized by systematical substitution at the aromatic backbone yielding the ligand $TMG5NMe_2asme$ (**L11***).[39] In 2019, tin(II) octoate was finally beaten for the first time by a N,O hybrid guanidine complex, however, not by a zinc complex but the iron complex [$Fe(TMG5NMe_2asme)Cl_2$].[40] It was found that this complex, exhibiting a rate constant of propagation that is about one order of magnitude higher than for tin(II) octoate, is able to polymerize lactide following pseudo first order kinetics and the coordination–insertion mechanism. In the following years it was demonstrated that because of the iron center, these complexes are also able to catalyze the atom transfer radical polymerization (ATRP) and are active in a combination of ROP and ATRP yielding novel copolymers.[41] Moreover, they can be used in the copolymerization of lactide with other cyclic esters, *e.g.* ε-caprolactone.[42] Initially studied for the zinc TMGasme complexes,[43] the complex [$Fe(TMG5NMe_2asme)Cl_2$] was further investigated in the alcoholysis and aminolysis as a chemical recycling method for PLA.[44] The catalyst depolymerizes PLA to methyl lactate (MeLA) in the presence of methanol at 60 °C within 24 h completely.

Overall, these thoroughly investigated iron(II) TMGasme complexes reveal the potential of iron guanidine complexes and these promising results are the motivation for this work. Although guanidine metal complexes have been a relevant topic for years, iron guanidine complexes were only investigated scarcely in the field of ROP. The present study can therefore draw from the whole library of known guanidine ligands. Aiming at inexpensive starting materials and a straightforward synthesis as well as a versatile ligand architecture, this work reports eight novel iron(II) chloride complexes **C1–C8** based on literature-known bisguanidine and N,N hybrid guanidine ligands **L1–L8** (see Fig. 1B). Their catalytic activity and polymerization behavior in the ROP of lactide are evaluated under industrially relevant conditions to identify the most promising catalysts which are then studied in more detail. Findings are further supported by density functional theory (DFT) calculations. Moreover, a selection of catalysts is applied in the methanolysis of PLA. Finally, the experimental observations are related in order to deepen the understanding of the connection between structural motives and the polymerization activity and stability of the catalysts.

Results and discussion

Iron(II) guanidine complexes

The eight ligands **L1–L8** were prepared following literature procedures in one step starting from the corresponding amine and the DMEG or TMG Vilsmeier reagent. Ligands **L1**,[45] **L2**,[46] **L7**[47] and **L8**[48] feature rigid aromatic backbones,

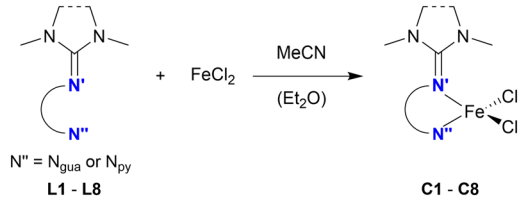

Scheme 1 Preparation of the iron(II) guanidine complexes starting from $FeCl_2$ and ligands **L1**–**L8** (gua = guanidine, py = pyridine). **C5** is an exception forming a complex cation with an iron center that is fivefold coordinated by two TMGpy (**L5**) ligands and one chlorido ligand.

while **L3**[35] and **L4**[33,35] possess an aliphatic backbone. **L5**[49] and **L6**[50] are guanidine–pyridine hybrid ligands. The complex syntheses were conducted under inert conditions with varying procedures depending on the complexes' solubility in acetonitrile (see Scheme 1). Especially complexes **C2**, **C3** and **C8** exhibit a straightforward preparation since they are hardly soluble in acetonitrile and precipitated as a powder upon formation. Complexes **C1**, **C5**, **C6** and **C7** were prepared by vapor diffusion of diethyl ether into a solution of the complex in acetonitrile and were obtained as crystalline solids. **C4** was prepared by layering a solution of the complex in acetonitrile with diethyl ether. The molecular structures of complexes **C1**–**C8** in the solid state were determined by single-crystal X-ray diffraction (see Fig. 2). Suitable single-crystals were either obtained directly from the crystallization *via* vapor diffusion (**C1**, **C5**, **C6** and **C7**) or were prepared by recrystallization from acetonitrile (**C2**, **C3**, **C4**, **C8**). Key geometric data of all complexes is summarized in Table 1.

The degree of delocalization (ρ) with values close to 1 indicates that the C=N double bond in all guanidine units of complexes **C1**–**C8** is fully delocalized. Except for **C5**, all iron centers are fourfold coordinated by two chlorido ligands and one bidentate N,N ligand. Complexes **C1**–**C4** and **C6**–**C8** possess a distorted tetrahedral coordination geometry as indicated by the τ_4 values,[51] with **C1** and **C2** being closest to a tetrahedral geometry and **C3** being most distorted with a τ_4 value of 0.73. The bite angles of the N,N ligands in the fourfold coordinated complexes **C1**–**C4** and **C6**–**C8** deviate strongly from the ideal tetrahedral angle of 109.47° with the strongest deviation for the ligands with C_2-spacers in their backbone (**C1**, **C3**, **C7**). Complex **C5** is an exception: the metal center is fivefold coordinated by two TMGpy (**L5**) ligands and one chlorido ligand. The second chloride anion is non-coordinating. The τ_5 value[52] of 0.68 indicates a strongly distorted trigonal bipyramidal coordination geometry. Both pyridine donor units are found in the apical positions, while the bulky TMG donor units and the chlorido ligand are located in the equatorial positions.

In the bisguanidine complexes **C2**–**C4** and **C7**, both $Fe–N_{gua}$ bond lengths are equal. Only **C1** and **C8** exhibit a slight difference in their two iron-guanidine bond lengths. In **C5** and **C6**, the $Fe–N_{TMG}$ bond lengths are clearly shorter than the $Fe–N_{py}$ bond lengths indicating a stronger donation through the TMG unit. Comparing complex **C1** with **C7** which are only different in their guanidine unit (TMG or DMEG), one of the $Fe–N_{TMG}$ bond lengths in **C1** is slightly longer than the $Fe–N_{DMEG}$ bond lengths in **C7**. One of the $Fe–N_{DMEG}$ bond lengths in **C8** is slightly shorter than the $Fe–N_{TMG}$ bond lengths in **C2**. Complex **C7**

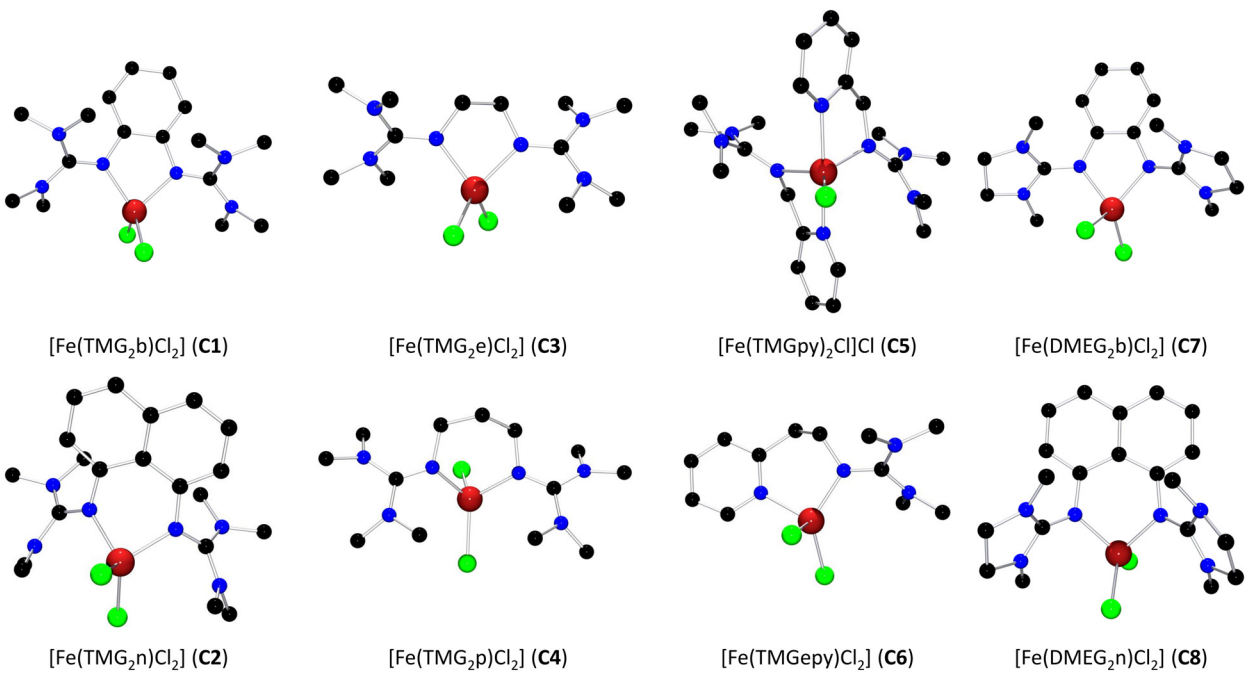

Fig. 2 Molecular structures of complexes **C1**–**C8** in the solid state. Hydrogen atoms and the non-coordinating chloride ion in **C5** were omitted for clarity.

Table 1 Key geometric data of complexes **C1–C8**

Complex	Fe–N_{gua} [Å]	Fe–$N_{gua,py}$ [Å]	N_{gua}–Fe–$N_{py/gua}$ [°]	ρ^a	$\tau_4{}^b/\tau_5{}^c$
C1	2.093(1)	2.068(1)	79.9(1)	0.98/0.98	0.89
C2	2.051(2)	2.052(2)	86.7(1)	0.98/0.99	0.90
C3	2.084(1)	2.084(1)	81.9(1)	0.96/0.96	0.73
C4	2.055(2)	2.054(1)	93.4(1)	0.97/0.97	0.81
C5	2.092(3)/2.072(2)	2.218(3)/2.213(3)	76.9(1)/75.8(1)	0.98/0.96	0.68
C6	2.021(3)	2.120(3)	94.5(2)	0.98	0.85
C7[d]	2.076(3)	2.073(3)	79.8(2)	0.99/1.01	0.88
	2.073(3)	2.073(3)	80.3(2)	0.97/0.97	0.88
C8	2.054(1)	2.036(1)	87.6(1)	0.97/0.99	0.84

[a] Degree of delocalization within the guanidine moiety: $\rho = 2a/(b + c)$ with $a = d(C{=}N_{gua})$ and b, $c = d(C{-}N_{amine})$.[48] [b] $\tau_4 = [360° - (\alpha + \beta)]/141°$.[51] α and β are the largest angles in a complex with a fourfold coordinated metal center. [c] $\tau_5 = (\beta - \alpha)/60°$.[52] α and β are the largest angles in a complex with a fivefold coordinated metal center with $\beta \geq \alpha$. [d] Two complex molecules are found in the asymmetric unit.

contains two independent complex molecules in the asymmetric unit with the major difference that the DMEG units are tilted into different directions.

All catalysts were examined by thermogravimetric analysis (TGA) at 150 °C for 1 h. Catalysts **C2–C8** proved to be thermally stable. The supposed sample of **C1** showed a mass loss of approximately 8% starting at about 125 °C. The IR spectra recorded before and after the TGA experiment differ due to loss of solvent molecules (see Fig. S11–S13†). Single-crystal X-ray diffraction data indicates that the acetonitrile solvate [Fe(TMG_2b)Cl_2]·1.5MeCN (**C1**·1.5MeCN) can also be obtained during crystallization. Due to the insufficient quality of the dataset, the structure of this acetonitrile solvate could not be solved properly. It was not possible to selectively crystallize one of the compounds.

Evaluation of polymerization activities

The melt polymerization of L-lactide with complexes **C1–C8** was conducted in a batch reactor on an 8 g-scale monitored by *in situ* Raman spectroscopy. Recrystallized L-lactide was employed in order to improve the reproducibility of the kinetics experiments. All experiments were conducted in duplicate at a monomer-to-initiator ratio ([M]/[I]) of 1000 : 1 at 150 °C under argon as inert gas. No additional co-initiator (CoI) was applied because zinc and iron guanidine complexes are known to function as single-site catalysts initiating through their nucleophilic guanidine ligands.[29,40] Polymerization times varied depending on the catalyst activity (see Table 2). For comparison, the polymerization was performed with anhydrous $FeCl_2$ as catalyst and an additional control experiment without catalyst can be found in the ESI† (see Fig. S40).

Two factors must be discussed: the activity as described by the initial apparent rate constant k_{app} and the stability of the complex meaning the time the polymerization activity is maintained before the activity decreases. The k_{app} values were determined from the semilogarithmic plots for each catalyst (see Fig. 3, all plots can be found in the ESI†). The k_{app} values of **C1–C8** differ drastically over four orders of magnitude (10^{-6}–10^{-3} s^{-1}). Therefore, the catalytic activity is compared with respect to the order of magnitude rather than the absolute k_{app} values.

Since the selective formation of one of the species of **C1** could not be controlled, the molar mass was assumed to be the molar mass of the acetonitrile-free species which may

Table 2 Results of the lactide polymerization with complexes **C1–C8** and $FeCl_2$[a]

Cat.	t [min]	p^b [%]	$k_{app}{}^c$ [10^{-4} s^{-1}]	$M_{n,theo}{}^d$ [kg mol^{-1}]	$M_n{}^e$ [kg mol^{-1}]	$Đ^e$
C1[f]	300	11	0.0629 ± 0.0047	15.9	n.d.[g]	n.d.[g]
C2	300	65	0.575 ± 0.073	93.7	25.0	1.5
C3	60	56	9.63 ± 0.05	80.7	25.3	1.5
C4	60	42	54.2 ± 14.1	60.5	14.1	1.5
C5	60	41	2.35 ± 0.27	59.1	11.0	1.4
C6	10	59	24.1 ± 0.2	85.0	47.3	1.4
C7	300	7	0.0280 ± 0.0001	10.1	n.d.[g]	n.d.[g]
C8	300	80	1.32 ± 0.02	115.3	45.7	1.5
$FeCl_2$	300	16	0.0786 ± 0.0085	23.1	n.d.[g]	n.d.[g]

[a] Conditions: bulk polymerization of recrystallized L-lactide, [M]/[I] = 1000 : 1, T = 150 °C, stirring speed: 260 rpm, experiments were conducted in duplicate. Conversion p, molar masses and dispersities are only given for one experiment per catalyst. All experiments are listed in the ESI.† [b] Conversion determined by ^{1}H NMR spectroscopy. [c] Initial apparent rate constant k_{app}, for details and all plots see ESI.† [d] $M_{n,theo}$ = [M]/[I]·M(LA)·p. [e] Determined by GPC with THF as eluent and a conventional calibration using polystyrene standards. Molar masses were corrected by a correction factor of 0.58.[24] [f] For this catalyst, the two different crystal structures **C1** and **C1**·1.5MeCN were obtained. The [M]/[I] ratio was calculated assuming the structure of **C1**. [g] Molar mass and dispersity were not determined because no precipitation from EtOH at 20 °C was observed.

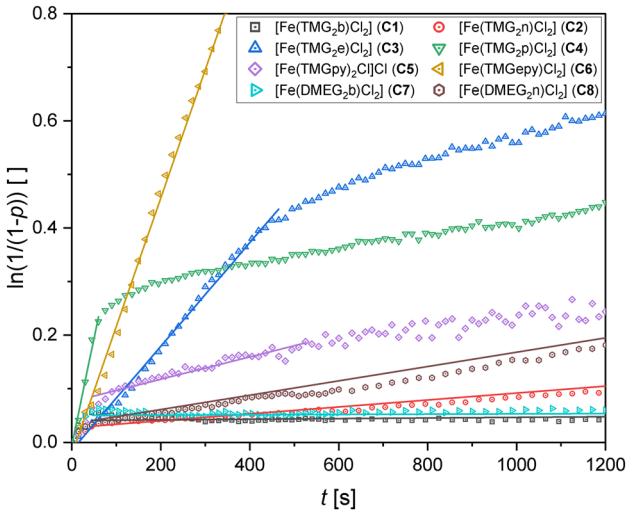

Fig. 3 Pseudo first order semilogarithmic plots for complexes **C1**–**C8** for the polymerization of recrystallized L-lactide (150 °C, [M]/[I] = 1000 : 1). Shown are the first 20 min of the experiments listed in Table 2. The plot for $FeCl_2$ is omitted for clarity. All plots can be found in the ESI.†

lead to slightly changed [M]/[I] ratios. This was, however, not further investigated because **C1** as well as **C7** exhibit very low polymerization activities comparable to $FeCl_2$ with k_{app} values in the order of magnitude of 10^{-6} s^{-1}. After 5 h, low conversions in the range of 10% were obtained and the product did not precipitate in ethanol meaning only short chains were formed. Due to the low activity and the comparably strong noise, no statement about the stability of the complexes can be made. The different guanidine units (TMG in **C1** and DMEG in **C7**) do not seem to change the rate constant drastically. Because of the very low activity, these two iron complexes are not suitable as catalysts for the ROP of lactide.

The complexes **C2** and **C8** containing a naphthalene backbone show a better activity with k_{app} values in the magnitude of 10^{-5} s^{-1} for **C2** and 10^{-4} s^{-1} for **C8**, respectively. Interestingly, for these two complexes only a slight decay of activity is observed after more than 1 h. Although they exhibit a mediocre activity, they follow pseudo first order kinetics. Comparing **C2** and **C8**, the change of the TMG groups to DMEG groups leads to a different activity, however, this effect is not as pronounced as for a change of the ligand backbone. The different activity is also reflected by the conversions after 5 h and the molar masses. Although these values show fluctuations, a general trend is observable. While **C2** reaches conversions of up to 65% and an M_n of 25.0 kg mol^{-1}, **C8** polymerizes the lactide to a conversion of 80% with an M_n of up to 45.7 kg mol^{-1}.

Compared to these four examples with aromatic ligand backbones, complexes **C3**–**C6** bearing aliphatic ligand backbones with two guanidine units (**C3**, **C4**) or a combination of one guanidine unit and a pyridine unit (**C5**, **C6**) show significantly higher initial k_{app} values. **C4** is the most active catalyst in the range of the complexes investigated in this work. However, it is also the complex with the shortest span of high activity of merely 1 min. Therefore, the experiment was repeated with sublimated L-lactide in order to evaluate the influence of lactide purity (see Fig. S52†). However, this did not change the polymerization rate significantly nor the short period of high activity. **C3** also shows a decay of activity but significantly later than **C4** with an initial k_{app} value similar to the second most active iron guanidine catalyst [Fe(TMGasme)Cl_2] and the industrially-applied $Sn(Oct)_2$ under comparable conditions (see Table 3 entries 1 and 3).[40] **C5** being the only five-coordinate complex in this study exhibits a rather mediocre activity with a curve-like semilogarithmic plot. Also, the polymers produced by this complex show the strongest deviation from the theoretical molar masses. This is likely due to the two ligand molecules per complex molecule that can function as an initiator and lead to a larger number of polymer chains compared to the other complexes containing only one ligand molecule per complex molecule. Although for all three complexes **C3**–**C5** the polymerization rate decreases

Table 3 Results from literature for the bulk polymerization of lactide with the zinc chloride analogs of **C1**–**C7** and other catalysts evaluated under industrially-relevant conditions

No.	Catalyst	[M]/[I]	t [h]	p [%]	k_{app} [10^{-4} s^{-1}]	M_n [kg mol^{-1}]	$Đ$	Ref.
1[a]	[Fe(TMGasme)Cl_2]	1000/1	0.5	66	7.18	96.7	1.3	Rittinghaus *et al.* 2019[40]
2[a]	[Fe(TMG5NMe$_2$asme)Cl_2]	1000/1	1.6 min	73	37.52	147.0	1.6	Rittinghaus *et al.* 2019[40]
3[a]	$Sn(Oct)_2$	1000/1	25 min	69	9.88	168.0	1.9	Rittinghaus *et al.* 2019[40]
4[b]	[Zn((*R*,*R*)-DMEG$_2$(1,2)ch)$_2$](OTf)$_2$·THF	1250/1	7.4 min	89	225	83.6	1.6	Hermann *et al.* 2020[29]
5[c]	[FeCp(CO)(trz)I]	1000/1	2	91	53.9 ± 4.1	21	2.5	Nylund *et al.* 2022[18]
6[d]	[Zn(TMG$_2$b)Cl_2]	500/1	48	80		7.0	2.09	Vieira 2013[55]
7[e]	[Zn(TMG$_2$n)Cl_2]	—	—	—		—	—	Reinmuth *et al.* 2009[54]
8[d]	[Zn(TMG$_2$e)Cl_2]	500/1	24	87		45.0 (M_w)	1.9	Börner 2009[56]
9[d]	[Zn(TMG$_2$p)Cl_2]	500/1	24	71		26.0 (M_w)	1.7	Börner 2009[56]
10[d]	[Zn(TMGpy)Cl_2]	1000/1	24	67		62.0 (M_w)	2.32	Börner *et al.* 2009[37]
11[d]	[Zn(TMGepy)Cl_2]	500/1	18	87	0.26	19.0	1.69	Vieira 2013[55]
12[d]	[Zn(DMEG$_2$b)Cl_2]·MeCN	500/1	48	67		4.0	1.79	Vieira 2013;[55] Roquette *et al.* 2011[57]

[a] Conditions: recrystallized L-lactide, 150 °C, same setup as in this work. [b] Conditions: *rac*-lactide, 150 °C, same setup as in this work. [c] *rac*-Lactide, 150 °C, trz: triazolylidene N-heterocyclic carbene ligand.[18] [d] *rac*-Lactide, 150 °C. [e] This complex was not evaluated in the polymerization of lactide.

over the course of the polymerization, a complete decay of activity was not observed. The final k_{app} values at the end of the polymerization time of 1 h are still in the range of 1×10^{-4} s^{-1} for **C3–C5** which is significantly higher than for $FeCl_2$. This indicates that a species different from the original iron complex is further supporting polymerization. This decrease of k_{app} during the polymerization process was also observed before for the zinc TMGasme systems and was attributed to the guanidine ligand functioning as an initiator for new growing polymer chains.[53]

The iron(II) N,N hybrid guanidine complex **C6** combines a high polymerization activity with stability. The experiments performed at an [M]/[I] ratio of 1000 : 1 lead to high conversions and no deactivation behavior was observed for this catalyst. After 10 min, the reaction had to be stopped due to the high viscosity causing fluctuations of the stirring speed. Conversions in the range of 60% and polymers with M_n values higher than 40 kg mol^{-1} could be obtained. Thus, this complex is the most promising catalyst in the scope of the herein investigated ROP catalysts and was therefore also investigated in detail (see below). In comparison to $Sn(Oct)_2$ and other robust iron catalysts that have been investigated under industrially relevant conditions (see Table 3 entries 1–3 and 5) the catalyst can keep up regarding the order of magnitude of k_{app} at an [M]/[I] ratio of 1000 : 1. However, it yields polymers with lower molar masses than several of the other examples. Possibilities to improve the molar masses and the dispersities are discussed below. The zinc guanidine complex $[Zn((R,R)\text{-}DMEG_2(1,2)ch)_2](OTf)_2 \cdot THF$ from a former publication is however still surpassing the activity by an order of magnitude (see Table 3 entry 4).

As already observed for the complexes $[Zn(TMG5NMe_2asme)Cl_2]$ and $[Fe(TMG5NMe_2asme)Cl_2]$ in previous studies, exchanging the metal ion can lead to a drastically changed polymerization activity.[38,40] Therefore, an intriguing comparison are the activities of the herein presented iron(II) guanidine complexes and the zinc chloride analogs that were investigated in the early stages of the research on metal guanidine catalysts for the ROP of lactide. The zinc chloride analogs of **C1–C7** are known and were, except of the **C2**-analog,[54] evaluated for the lactide polymerization (see Table 3 entries 6–12). Although the polymerization method in these early publications deviates considerably from the polymerization applied in this work the polymerization results for the six complexes $[Zn(TMG_2b)Cl_2]$,[55] $[Zn(TMG_2e)Cl_2]$,[56] $[Zn(TMG_2p)Cl_2]$,[56] $[Zn(TMGpy)Cl_2]$,[37] $[Zn(TMGepy)Cl_2]$[55] and $[Zn(DMEG_2b)Cl_2]\cdot MeCN$[55,57] illustrate which enormous effect the replacement of a zinc to an iron center can have. While this is not obvious for the zinc chloride analogs of **C1** and **C7** (see Table 3 entries 6 and 12) because **C1** and **C7** show a low activity by themselves, the difference becomes apparent for the other iron complexes **C3–C6**. The polymerizations with the zinc complexes had to be conducted for several hours up to days at 150 °C and were carried out with higher catalyst concentrations ([M]/[I] = 500 : 1) in order to achieve high conversions. However, the long polymerization times were accompanied by broad molar mass distributions.

To have a more comparable result, the polymerization with **C3** was repeated using a [M]/[I] ratio of 500 : 1 (see Table 4 entry 1). After merely 1 h, a conversion of 80% was obtained while the zinc chloride analog requires 24 h for a conversion of 87% (see Table 3 entry 8). Moreover, $[Zn(TMGepy)Cl_2]$, the zinc analog of **C6**, exhibits a much decreased activity with a k_{app} value of merely 2.6×10^{-5} s^{-1} at an [M]/[I] ratio of 500 : 1[55] while **C6** exhibits a k_{app} value that is two orders of magnitude higher at an even lower catalyst concentration ([M]/[I] = 1000 : 1, see Table 2). This comparison again highlights the potential of iron-based catalysts for the ROP of lactide.

Experiments on extending the duration of high activity with $[Fe(TMG_2e)Cl_2]$ (C3)

In order to gain deeper insight into the interplay of the iron center and the ligand and to extent the duration of high

Table 4 Additional polymerization experiments with **C3** and **C6**[a]

No.	Cat.	CoI/ additive	[M]/[I]/[CoI]	t [min]	p^b [%]	$k_{app}{}^c$ [10^{-4} s^{-1}]	$M_{n,theo}{}^d$ [kg mol^{-1}]	$M_n{}^e$ [kg mol^{-1}]	$Đ^e$
1	**C3**	—	500/1/—	60	80	14.8	57.7	46.2	1.4
2	**C3**	—	1000/1/—	60	56	9.67	80.7	25.3	1.5
3	$FeCl_2$	TMG_2e (**L3**)	1000/1/—	60	25	1.22	36.0	3.0	1.2
4	**C3**	*p*MeBnOH	1000/1/1	60	63	10.1	45.4	33.7	1.2
5	**C3**	$FeCl_2$	1000/1/1	60	76	8.79	109.5	67.7	1.5
6	**C3**	TMG_2e (**L3**)	1000/1/1	60	45	19.8	64.9	8.1	1.4
7	**C6**	—	2000/1/—	60	44	8.47	126.8	29.9	1.5
8	**C6**	*p*MeBnOH	2000/1/1	60	68	17.8	98.0	68.3	1.4
9	**C6**	*p*MeBnOH	2000/1/4	60	75	27.8	43.2	48.7	1.3
10	**C6**	*p*MeBnOH	5000/1/5	60	34	6.02	40.8	26.9	1.2
11	**C6**	$FeCl_2$	2000/1/1	60	65	11.0	187.4	68.5	1.4

[a] Conditions: bulk polymerization of recrystallized L-lactide, T = 150 °C, stirring speed: 260 rpm. [b] Conversion determined by ^1H NMR spectroscopy. [c] Initial apparent rate constant k_{app}, for details and all plots see ESI.† [d] $M_{n,theo}$ = [M]/([CoI] + [**C3**/**C6**])·M(LA)·p. $FeCl_2$ was not considered as a co-initiator. [e] Determined by GPC with THF as eluent and a conventional calibration using polystyrene standards. Molar masses were corrected by a correction factor of 0.58.[24]

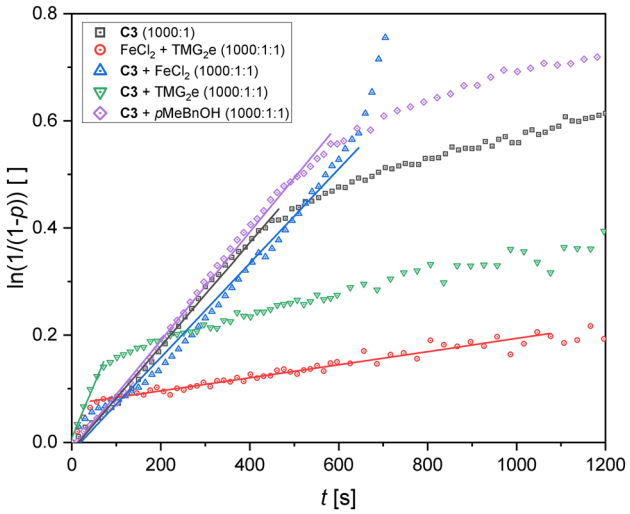

Fig. 4 Pseudo first order semilogarithmic plots for the polymerization of recrystallized L-lactide with **C3** and various additives. For comparison, the polymerization without additive is depicted ([M]/[I] = 1000 : 1). Shown are the first 20 min of the experiments. Full plots can be found in the ESI.†

activity, additional experiments with **C3** were conducted (see Fig. 4 and Table 4 entries 1–6). This catalyst was chosen because of its comparably high activity, its straightforward preparation and the solid ligand TMG_2e (**L3**). Firstly, the *in situ* formation of the catalyst was tested by adding solid $FeCl_2$ and **L3** to the L-lactide (see Table 4 entry 3). However, the resulting k_{app} value of 1.22×10^{-4} s^{-1} measures only one eighth compared to the iron(II) complex **C3** ([M]/[I] = 1000 : 1, see Table 4 entry 2). Given the fact that $FeCl_2$ and **L3** on their own exhibit very low k_{app} values in the magnitude of 10^{-6} s^{-1} for [M]/[I] = 1000 : 1 (see Table 2 and Fig. S45†), this result shows that the activity must be caused by the complex **C3**. Moreover, the determined k_{app} value is similar to the k_{app} value obtained for the complex **C3** after the decrease of activity. Therefore, small proportions of complex might be formed *in situ* in the lactide melt and/or the same species forms that forms after the decay of activity in the polymerization with **C3**.

Since the addition of a co-initiating alcohol is common in literature, an additional polymerization experiment with 1 equivalent of *p*-methyl benzyl alcohol (*p*MeBnOH) was performed ([M]/[I]/[*p*MeBnOH] = 1000 : 1 : 1, see Table 4 entry 4). Indeed, the addition of alcohol leads to a modest improvement with a slightly increased conversion and a higher molar mass with a lower dispersity after 1 h at 150 °C. Surprisingly, the addition of 1 equivalent of ligand **L3** does not result in a better polymerization performance (see Table 4 entry 6). In the first minute, the rate is increased compared to the experiment without additional ligand. However, afterwards the rate is significantly lower. Therefore, additional ligand might function as a co-initiator to some extent but at the same time it acts as a deactivator probably by coordination to the iron center. However, such a species could not be isolated since in crystallization experiments with 2 equivalents of **L3** only **C3** was obtained. The addition of 1 equivalent of $FeCl_2$ to the polymerization mixture leads to the highest conversion after 1 h (76%) which indicates that the oxidation of iron(II) might be a problem and can be partially suppressed by additional iron(II) salt (see Table 4 entry 5). The molar mass is also significantly increased to 67.7 kg mol^{-1} compared to 25.3 kg mol^{-1} for the experiment without $FeCl_2$. However, the addition of $FeCl_2$ does not lead to a higher initial k_{app}, the high activity is merely maintained for a longer time.

In-detail investigation of the polymerization behavior of [Fe(TMGepy)Cl_2] (C6)

Since **C6** showed the most promising activity with high conversions within minutes, the polymerization behavior of this ROP catalyst was investigated further. First the [M]/[I] ratio was varied at 150 °C between 1000 : 1 and 5000 : 1 in order to determine the concentration-independent rate constant of propagation k_p. In this context, it was also found that at [M]/[I] ratios higher than 1000 : 1 a decay of activity is also observed for **C6** (see Fig. S47–S51†). The determined initial k_{app} values were plotted against the catalyst concentration [I] and a regression line was determined showing that the reaction is well in accordance with a pseudo first order mechanism (see Fig. 5). The slope of the regression line provides a k_p value of (0.365 ± 0.004) L mol^{-1} s^{-1}. This value is in the same order of magnitude as for [Fe(TMG5NMe$_2$asme)Cl_2] being one of the to-date most active robust iron catalysts with a k_p value of (0.554 ± 0.02) L mol^{-1} s^{-1}.[40] However, the one-step preparation of **L6** proves to be straightforward and more efficient compared to the four-step synthesis of $TMG5NMe_2asme$ (**L11***).

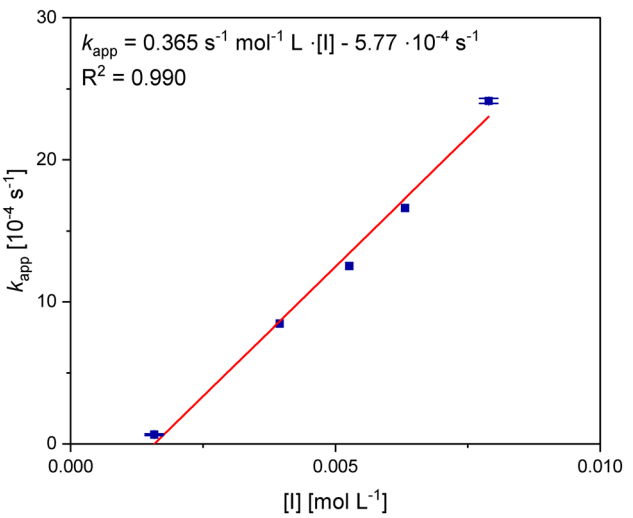

Fig. 5 Plot of k_{app} *vs.* the catalyst concentration [I] for the determination of k_p for **C6** at 150 °C. The end points were determined in duplicate ([M]/[I] = 1000 : 1 and 5000 : 1). The error bars show the standard deviation of the two experiments.

Increasing the polymerization temperature to 180 °C leads to a doubling of the initial k_{app} value (39.8×10^{-4} s^{-1} for 180 °C *vs.* $(24.1 \pm 0.2) \times 10^{-4}$ s^{-1} for 150 °C with [M]/[I] = 1000 : 1, see Fig. S55†). Lowering the temperature to 135 °C has an even more drastic effect with a conversion of only 16% after 10 min compared to 59% for 150 °C (see Fig. S54†). This highlights the importance of an appropriate polymerization temperature when applying the presented iron(II) guanidine catalysts. Additional experiments were performed with sublimated L-lactide and technical-grade *rac*-lactide with an [M]/[I] ratio of 2000 : 1 at 150 °C (see Fig. S57 and S58†). With increasing degree of purification, the k_{app} value rises from 6.89×10^{-4} s^{-1} (technical grade *rac*-lactide) to 1.14×10^{-3} s^{-1} (sublimated L-lactide) which is likely due to the purity.

In order to lower the catalyst loading, experiments with the co-initiator *p*MeBnOH were conducted (see Fig. 6 and Table 4 entries 8–10). Adding *p*MeBnOH generally leads to higher initial k_{app} values, lower dispersities and can improve the molar masses at high [M]/[I] ratios. This is most pronounced for experiments with very low catalyst concentrations. While for the experiment without co-initiator at [M]/[I] = 5000/1 no polymer could be precipitated from ethanol (see Table S7†), for [M]/[I]/[*p*MeBnOH] = 5000/1/5 polymer with an M_n of 26.9 kg mol^{-1} and a dispersity of 1.2 was obtained (see Fig. 6 and Table 4 entry 10). This illustrates that an alcohol such as *p*MeBnOH can be used as an inexpensive instrument to both lower the catalyst loading as well as improve the polymerization rate and polymer properties. The co-initiator is functioning as a nucleophile that initiates new growing chains. These observations are also in accordance with a former study on a zinc N,O hybrid guanidine complex.[53] Analogous to **C3**, an experiment with the addition of 1 equivalent of $FeCl_2$ was conducted ([M]/[I]/[$FeCl_2$] = 2000 : 1 : 1, see Fig. 6 and Table 4 entry 11). Again, a longer linear behavior was observed and a significantly higher molar mass was obtained after 1 h at 150 °C compared to the experiment without $FeCl_2$ (see Table 4 entry 7).

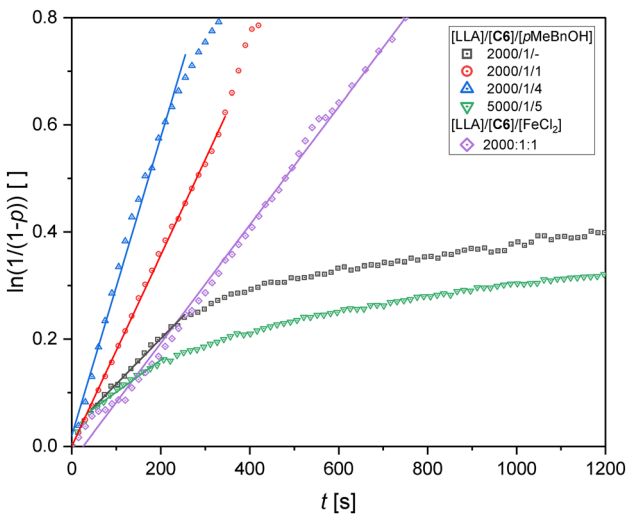

Fig. 6 Pseudo first order semilogarithmic plots for the polymerization with **C6** and co-initiator *p*MeBnOH as well as the polymerization with **C6** and $FeCl_2$. For comparison, the polymerization without co-initiator is depicted ([M]/[I] = 2000 : 1). Shown are the first 20 min of the experiments. Full plots can be found in the ESI.†

MALDI-TOF mass spectra of polymer produced with **C6** with an [M]/[I] ratio of 100 : 1 showed that the ligand TMGepy (**L6**) can be an end group (see Fig. S66†). This highlights the underlying coordination–insertion mechanism and the nucleophilicity of guanidine ligands. Additionally, in an experiment where *p*MeBnOH was applied as co-initiator ([M]/[I]/[*p*MeBnOH] = 100 : 1 : 1, see Fig. S67†), co-initiator was also found as end group. These observations are in accordance with the polymerization with other zinc and iron guanidine catalysts.[38,40]

The thermal properties of the poly-L-lactide produced by **C6** with and without co-initiator were investigated by DSC (see Table S10†). The resulting glass transition temperatures in the range of 60 °C and melting peaks in the range of 170 °C are consistent with literature values for poly-L-lactide.[2]

DFT calculations

To understand the very different polymerization activities of **C1–C8**, DFT calculations were conducted (see Table 5). The functional TPSSh[58,59] and the basis set def2-TZVP[60–62] with a solvent model for MeCN using the polarizable continuum model (PCM) and an empirical dispersion correction using the D3 version of Grimme's dispersion with Becke–Johnson damping (GD3BJ)[63–65] were applied. The optimized structures are in good accordance with the experimentally determined solid state structures as indicated by the low root mean-square deviations (RMSD values) and the comparison of the characteristic bond lengths and structure parameters (see Tables S14 and S15†). All calculations were carried out for the high-spin state (quintet) since the Fe–N bond lengths are in the typical range of high-spin iron complexes.

The structural optimization calculations were followed by natural bond orbital (NBO) calculations.[66,67] The NBO charges of the iron centers in complexes **C1–C8** only cover a small range between +1.23 and +1.30. Moreover, the NBO charges do not match the polymerization activities, and therefore, the Lewis acidity of the metal center cannot be the only factor influencing the catalytic activity. However, the charge-transfer energies between the N and Cl donor atoms, respectively, and the iron center can contribute to an explanation of the different activities and also stabilities. The complex cation **C5#** is only scarcely considered in the following discussion because of its significantly different structure, and therefore, a very limited comparability to the other complexes **C1–C4** and **C6–C8**.

Complexes **C3**, **C4** and **C6** turned out to be the most active catalysts with the highest k_{app} values in the experimental studies (see above). The DFT calculations show that these

Table 5 Computational results for the complexes **C1**–**C8** and the complex [Fe(TMGqu)Cl_2] (**C9***) from a former work[40] (NBO 7.0, TPSSh/def2-TZVP, GD3BJ, PCM (MeCN))[a]

	NBO charges [e units]					Charge-transfer energies [kcal mol^{-1}]					
Complex	Fe	$N_{gua,1}$	$N_{gua,2/py/qu}$	Cl_1	Cl_2	$N_{gua,1}$ → Fe	$N_{gua,2/py/qu}$ → Fe	∅(N → Fe)	Cl_1 → Fe	Cl_2 → Fe	∅(Cl → Fe)
C1	1.25	−0.69	−0.69	−0.74	−0.75	42.0	42.1	42.1	93.3	85.5	89.4
C2	1.24	−0.71	−0.70	−0.72	−0.75	47.1	47.4	47.3	100.2	83.8	92.0
C3	1.24	−0.69	−0.69	−0.75	−0.75	49.1	49.1	49.1	84.8	84.8	84.8
C4	1.28	−0.70	−0.70	−0.75	−0.76	43.3	43.2	43.3	83.3	80.4	81.9
C5#[b]	1.30	−0.68/−0.68	−0.52/−0.52	−0.72	—	47.7/47.2	40.0/39.9	43.9/43.6	95.4	—	95.4
C6	1.27	−0.71	−0.54	−0.73	−0.77	52.3	41.4	46.9	95.4	76.0	85.7
C7	1.24	−0.71	−0.71	−0.74	−0.74	38.8	39.0	38.9	90.3	90.3	90.3
C8	1.23	−0.71	−0.71	−0.72	−0.75	44.8	47.4	46.1	97.5	86.8	92.2
C9*	1.26	−0.69	−0.51	−0.73	−0.74	41.2	42.7	42.0	96.7	88.5	92.6

[a] Further details and calculated values as well as RMSD values can be found in Table S14.† [b] Calculation was performed for the complex cation $[Fe(TMGpy)_2Cl]^+$ (**C5#**).

three complexes with an aliphatic ligand backbone exhibit lower Cl → Fe charge-transfer energies compared to the less active complexes **C1**, **C2**, **C7** and **C8** with an aromatic ligand backbone. To further illustrate this relation, the k_{app} values at [M]/[I] = 1000 : 1 were plotted *versus* the average charge-transfer energies of the two Fe–Cl bonds (see Fig. 7). A low Cl → Fe charge-transfer energy is probably essential for the lactide coordination since the peralkylated guanidine donor units are sterically demanding and to enable the coordination of a lactide molecule as well as the growing polymer chain, the cleavage of an Fe–Cl bond might be necessary.

The second factor relevant for the overall catalyst performance is the catalysts' ability to maintain the controlled polymerization behavior following pseudo first order kinetics over time. This stability seems to be linked to the strength of the Fe–N bonds. Complexes **C2**, **C3**, **C6** and **C8** exhibit the highest values for the N → Fe charge-transfer energies. The strong Fe–N_{gua} bonds explain the much higher stabilities of **C3** and **C6** compared to complex **C4**, which possesses rather weak N–Fe bonds and looses its high activity already after the first minute of polymerization. Moreover, the comparatively high N → Fe charge-transfer energies explain the steady polymerization activity of complexes **C2** and **C8** based on ligands with naphthalene backbones. Additionally, the much stronger electron density donation through a guanidine donor compared to a pyridine donor becomes apparent in the calculated N → Fe charge-transfer energies as can be seen for the hybrid guanidine complexes **C5** and **C6**. This might be an additional reason for the good activity of hybrid guanidine complexes: the guanidine is tightly bound to the metal center while the second donor unit, the pyridine unit, can be more easily replaced by an approaching lactide molecule.

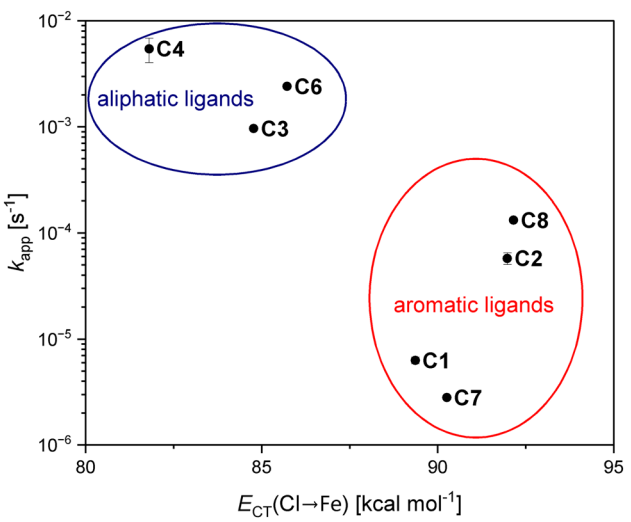

Fig. 7 Plot of the experimental initial k_{app} values ([M]/[I] = 1000 : 1, 150 °C) *vs.* the average Cl → Fe charge transfer energy (E_{CT}(Cl → Fe)) in complexes **C1**–**C4** and **C6**–**C8**. The complex cation **C5#** was omitted because it is not comparable to the other complexes. The error bars are partially invisible due to too small error values.

The combination of both influences on the catalyst performance, the Cl → Fe and the N → Fe charge transfer-energies, explains the very low polymerization activities of complexes **C1** and **C7**. In these complexes with an aromatic ligand backbone, the N_{gua}–Fe bonds are weakened in comparison to the other complexes, while the Fe–Cl bonds are strong leading to an activity in the order of magnitude of $FeCl_2$. Therefore, these complexes unite the features that are opposite to the trends found for suitable polymerization catalysts. This is also true for the iron(II) guanidine–quinoline complex [Fe(TMGqu)Cl_2] (**C9***) that has been investigated in the polymerization of technical-grade *rac*-lactide before and showed a very low polymerization activity with a k_{app} value of 3×10^{-6} s^{-1} at an [M]/[I] ratio of 500 : 1.[40] All DFT results considered, it can be concluded that for an active and stable catalyst a weak Fe–Cl bond as well as strong Fe–N bonds are required. An aliphatic ligand backbone is beneficial for a high activity. Complexes **C3** and **C6** combine these features explaining their outstanding polymerization performances. These findings will support the future design of iron(II) guanidine catalysts.

Table 6 Results of methanolysis experiments with complexes C2–C6[a]

Cat.	t [h]	X_{int}[b] [%]	S_{MeLA}[b] [%]	Y_{MeLA}[b] [%]	k_{app}[c] [min^{-1}]
C2	24	69	52	36	n.d.[d]
C3	3	100	93	93	0.0264 ± 0.0023
C4	3	99	82	81	0.0306 ± 0.0010
C5	0.25	100	100	100	n.d.[e]
C6	3	67	42	28	0.0050 ± 0.0005

[a] Conditions: 250 mg PLA (bio-mi Ltd., M_n = 46.7 kg mol^{-1}, $Đ$ = 1.5), 1 mol% catalyst (regarding the PLA ester bonds), methanol (7.13 equiv.), THF (4 mL), T = 60 °C, stirring speed: 260 rpm. For every catalyst, only one experiment is shown. The results of the other experiments can be found in Table S13.† [b] The conversion of internal methine groups of PLA (X_{int}), the selectivity towards the product methyl lactate (S_{MeLa}) and the yield of the product (Y_{MeLa}) were calculated from the ^{1}H NMR spectrum according to literature.[20] [c] Determined from the plot of ln([Int]$_0$/[Int]$_t$) *vs.* *t*. The average value with standard deviation is shown. [d] The depolymerization proceeds very slowly and the semilogarithmic plot is not in good accordance with a pseudo first order reaction. Therefore, k_{app} was not determined. [e] The depolymerization proceeds very rapidly. Therefore, the k_{app} value was not determined.

PLA depolymerization with the complexes C2–C6

Besides the research on the PLA synthesis *via* a ROP, the chemical recycling of PLA becomes more and more important in order to integrate the material into the circular economy approach. Therefore, and to investigate whether the trend found for the polymerization can be transferred to the depolymerization, initial tests using **C2–C6** for the methanolysis of PLA were performed (see Table 6). Choosing the same conditions as in previous publications[43,44] allows a comparison of **C2–C6** with other catalysts: PLA was depolymerized at 60 °C using 1 mol% catalyst, 7.13 equivalents MeOH and THF as solvent. The conversion of internal methine groups (X_{int}), the selectivity towards methyl lactate (MeLA) (S_{MeLA}) and the yield (Y_{MeLA}) were calculated. The apparent rate constants (k_{app}) were determined from the semilogarithmic plots assuming pseudo first order kinetics (see Fig. S68–S70†).[68]

As for the polymerization, **C2** shows a low activity with a maximum conversion of only 69% after 24 h and the kinetics deviated from a pseudo first order reaction. Therefore, no k_{app} value was determined for this complex. **C6** being the most promising ROP catalyst features a similar conversion (X_{int} = 67%) within 3 h reaching a methyl lactate yield of 28%. With a k_{app} of 0.0050 ± 0.0005 min^{-1} it has a comparable activity to [Fe(TMG5NMe$_2$asme)Cl$_2$] with a k_{app} of 0.0048 min^{-1} under the same reaction conditions.[44] The complete depolymerization of PLA to methyl lactate could not be observed (see Fig. S70†). **C3** and **C4** are an order of magnitude faster with k_{app} values of 0.0264 ± 0.0023 min^{-1} and 0.0306 ± 0.0010 min^{-1}, respectively (see Fig. S68 and S69†). High methyl lactate yields are reached within 3 h. Complex **C5** features an extraordinary activity being able to convert PLA completely to methyl lactate within 15 min. Overall, these experiments allow no correlation of the catalytic activities of the investigated complexes for the polymerization of lactide and the methanolysis of PLA. Due to the promising first results, further in-detail research will be conducted concerning the depolymerization abilities of the presented iron(II) guanidine catalysts and the structure–activity relationships.

Conclusion

In this study, eight well-known bisguanidine and N,N hybridguanidine ligands were reactivated showing the potential of their iron(II) chloride complexes **C1–C8**. Although ligands with a straightforward topology were chosen, they cover a wide range of structural motives with varying distances between the donor units, two types of the guanidine donor units and a different second donor unit in case of two guanidine–pyridine hybrid complexes. Except for one five-coordinate complex (**C5**) all complexes are four-coordinate with a distorted tetrahedral coordination geometry.

All complexes were evaluated in the melt polymerization of L-lactide under industrially relevant conditions revealing substantial differences in their activities and stabilities. However, they generally exhibit faster polymerization rates than their zinc chloride analogs that have been studied before. The complexes with aromatic ligand backbones (**C1**, **C2**, **C7** and **C8**) show low to mediocre activities rendering them unsuited for the application as ROP catalysts. On the contrary, the bisguanidine complexes **C3** and **C4** with an aliphatic ligand backbone exhibit a high initial activity. For **C4** this activity decreased drastically after the first minute, while **C3** is able to maintain its high activity for a longer time. The high activity phase of **C3** could be further extended by the addition of $FeCl_2$ improving conversion and molar masses. The N,N hybrid guanidine complex **C6** stood out with its ability to polymerize lactide within minutes to molar masses of more than 40 kg mol^{-1}. The catalyst loading could be successfully lowered by the use of a co-initiating alcohol, yielding polymers with even higher molar masses and low dispersities.

DFT calculations suggested that the strength of the Fe–Cl bond in iron(II) chloride guanidine complexes might be one of the main reasons for a catalyst's activity. At the same time, these calculations allowed to explain the decay of activity over time for some complexes by their decreased strength of the Fe–N bonds.

In addition to the polymerization study, first experiments regarding the methanolysis of PLA were conducted with

complexes **C2–C6**. Especially complex **C5** depolymerizes PLA to methyl lactate within minutes demonstrating the potential of these compounds for a circular use of PLA. Overall, this work provides new impetus for the research on iron guanidine complexes as polymerization catalysts and illustrates that the combination of well-known and easily prepared ligands with other metal precursors can unlock a previously unknown potential. This brings non-toxic catalysts for bioplastics closer to industrial application.

Experimental

Materials

All manipulations involving air- and/or moisture-sensitive materials were conducted under nitrogen or argon as inert gas applying standard Schlenk-techniques or in a nitrogen-filled glovebox. The glassware was dried at 150 °C and assembled while hot. Solvents used for the preparation of the iron complexes were purchased in analytical grade and were purified and degassed before use according to standard procedures.[69] Acetonitrile was distilled over CaH_2 and degassed by three freeze–pump–thaw cycles. Diethyl ether was distilled over sodium and degassed by three freeze–pump–thaw cycles. Anhydrous iron(II) chloride (purity 99.5%) was purchased from Alfa Aesar. L-Lactide (Lumilact L polymer grade, stereochemical purity ≥99.5%, free acid ≤7 meq kg^{-1}, water ≤0.03%) was donated by TotalEnergies Corbion and was recrystallized from toluene and stored in a nitrogen-filled glovebox at room temperature. *p*-Methyl benzyl alcohol (4-methyl benzyl alcohol, *p*MeBnOH) was purchased from TCI Deutschland and was recrystallized from toluene. PLA film (M_n = 46.7 kg mol^{-1}, $Đ$ = 1.5) for the depolymerization experiments was provided by bio-mi Ltd. (Matulji, Croatia). Methanol (Acros Organics, 99.8%, extra dry over molecular sieves) was degassed and stored over molecular sieves.

The guanidine ligands TMG_2b (**L1**),[45] TMG_2n (**L2**),[46] TMG_2e (**L3**),[35] TMG_2p (**L4**),[35] TMGpy (**L5**),[49] TMGepy (**L6**),[50] $DMEG_2b$ (**L7**)[47] and $DMEG_2n$ (**L8**)[48] were synthesized according to literature starting from the respective amine and the tetramethyl or dimethylethylene Vilsmeier reagent.

Preparation of iron(II) chloride guanidine complexes

[Fe(TMG$_2$b)Cl$_2$]/[Fe(TMG$_2$b)Cl$_2$]·1.5MeCN (C1/C1·1.5MeCN). Inside a nitrogen-filled glovebox, anhydrous iron(II) chloride (63 mg, 0.50 mmol, 1.0 equiv.) was dissolved in acetonitrile (3 mL) under heating. The resulting solution was added to the ligand TMG_2b (**L1**, 152 mg, 0.500 mmol, 1.00 equiv.). The mixture was shaken until a green solution formed (*circa* 1 min). The solution was filtered. By vapor diffusion of diethyl ether, green crystals (105 mg, 0.244 mmol, 49% yield calculated assuming the acetonitrile-free crystal structure **C1**) formed over the course of 1 week. Single-crystal X-ray diffraction yielded two different crystal structures which formed under the same crystallization conditions. However, the acetonitrile-containing structure **C1**·1.5MeCN could not be resolved due to the limited quality of the dataset.

IR for species without MeCN (**C1**) (crystals that were used for SC-XRD): IR (ATR, $\tilde{\nu}$) = 2936 (w, $\nu(CH_{aliph})$), 2932 (w, $\nu(CH_{aliph})$), 2878 (w, $\nu(CH_{aliph})$), 2798 (w, $\nu(CH_{aliph})$), 1577 (w), 1540 (vs, $\nu(C{=}N_{gua})$), 1534 (vs, $\nu(C{=}N_{gua})$), 1518 (vs, $\nu(C{=}N_{gua})$), 1481 (s), 1460 (m), 1446 (w), 1434 (w), 1417 (vs), 1406 (vs), 1392 (vs), 1334 (s), 1286 (w), 1271 (w), 1239 (m), 1210 (m), 1155 (vs), 1149 (vs), 1108 (w), 1065 (w), 1030 (vs), 948 (w), 931 (w), 869 (w), 837 (s), 817 (s), 798 (m), 770 (vs), 748 (vs), 710 (m), 637 (m), 624 (w), 566 (m), 508 (w) cm^{-1}. IR for acetonitrile-containing species (**C1**·1.5MeCN) (before TGA): IR (ATR, $\tilde{\nu}$) = 2934 (w, $\nu(CH_{aliph})$), 2873 (w, $\nu(CH_{aliph})$), 2801 (vw, $\nu(CH_{aliph})$), 1581 (w), 1557 (m), 1538 (s, $\nu(C{=}N_{gua})$), 1520 (vs, $\nu(C{=}N_{gua})$), 1484 (m), 1464 (m), 1448 (w), 1436 (w), 1420 (s), 1408 (vs), 1402 (vs), 1396 (vs), 1334 (m), 1292 (w), 1288 (w), 1272 (w), 1238 (w), 1212 (w), 1187 (vw), 1162 (m), 1155 (m), 1147 (m), 1114 (w), 1066 (w), 1058 (vw), 1039 (w), 1029 (s), 960 (vw), 937 (vw), 923 (w), 875 (w), 843 (m), 818 (s), 797 (w), 746 (vs), 704 (w), 631 (w), 623 (w), 577 (vw), 563 (m), 513 (w), 510 (w), 477 (vw) cm^{-1}. HR-MS (ESI+, MeCN), *m*/*z* (%): isotopic distribution calculated for $[C_{16}H_{28}Cl_2FeN_6]^+$ $[M]^+$: 428.11432 (6) $[C_{16}H_{28}{}^{35}Cl_2N_6{}^{54}Fe]^+$, 429.11767 (1) $[C_{15}{}^{13}CH_{28}{}^{35}Cl_2N_6{}^{54}Fe]^+$, 430.10964 (100) $[C_{16}H_{28}{}^{35}Cl_2N_6Fe]^+$, 431.11300 (17) $[C_{16}{}^{13}CH_{28}{}^{35}Cl_2N_6Fe]^+$, 432.10670 (64) $[C_{16}H_{28}{}^{35}Cl^{37}ClN_6Fe]^+$, 433.11005 (11) $[C_{16}{}^{13}CH_{28}{}^{35}Cl^{37}ClN_6Fe]^+$, 434.10374 (10) $[C_{16}H_{28}{}^{37}Cl_2N_6Fe]^+$, 435.10710 (2) $[C_{15}{}^{13}CH_{28}{}^{37}Cl_2N_6Fe]^+$; found: 430.10920 (100), 431.11188 (21), 432.10638 (62); isotopic distribution calculated for $[C_{16}H_{28}ClFeN_6]^+$ $[M–Cl]^+$: 393.14546 (6) $[C_{16}H_{28}{}^{35}Cl{}^{54}FeN_6]^+$, 395.14079 (100) $[C_{16}H_{28}{}^{35}ClFeN_6]^+$, 396.14415 (17) $[C_{15}{}^{13}CH_{28}{}^{35}ClFeN_6]^+$, 397.13784 (32) $[C_{16}H_{28}{}^{37}ClFeN_6]^+$; found: 393.14394 (8), 395.14037 (100), 396.14296 (20), 397.13758 (31).

[Fe(TMG$_2$n)Cl$_2$] (C2). Inside a nitrogen-filled glovebox, anhydrous iron(II) chloride (63 mg, 0.50 mmol, 1.0 equiv.) was dissolved in acetonitrile (4 mL) under heating. This solution was passed through a filter into a solution of the ligand TMG_2n (**L2**, 177 mg, 0.500 mmol, 1.00 equiv.) in acetonitrile (4 mL). Immediately, an orange precipitate formed. The mixture was shaken (*circa* 1 min). After settling, the supernatant was removed and the remaining solid was washed with diethyl ether (3 × 4 mL). After removing the volatile compounds under reduced pressure, the product $[Fe(TMG_2n)Cl_2]$ (**C2**, 219 mg, 0.455 mmol, 91% yield) was obtained as an orange powder. Single crystals suitable for single-crystal X-ray diffraction were obtained by recrystallization from acetonitrile.

IR (ATR, $\tilde{\nu}$) = 3009 (vw, $\nu(CH_{arom})$), 2954 (w, $\nu(CH_{aliph})$), 2924 (w, $\nu(CH_{aliph})$), 2887 (w, $\nu(CH_{aliph})$), 2862 (w, $\nu(CH_{aliph})$), 2789 (vw, $\nu(CH_{aliph})$), 1549 (s), 1538 (s), 1517 (vs, $\nu(C{=}N_{gua})$), 1503 (vs), 1463 (m), 1440 (w), 1415 (s), 1406 (s), 1398 (vs), 1378 (vs), 1343 (m), 1328 (s), 1278 (m), 1232 (m), 1176 (vw), 1159 (vs), 1145 (m), 1127 (w), 1115 (w), 1103 (w), 1064 (m), 1060 (m), 1017 (vs), 996 (vs), 976 (w), 959 (vw), 927 (w), 920 (w), 847 (vs), 807 (vs), 786 (s), 768 (vs), 754 (s), 691 (s), 667 (vw), 624 (m), 576 (vw), 545 (w), 526 (vw), 508 (m), 480 (w),

475 (w), 412 (vw), 410 (vw) cm^{-1}. HR-MS (ESI+, MeCN), *m/z* (%): isotopic distribution calculated for $[C_{20}H_{30}Cl_2FeN_6]^+$ $[M]^+$: 478.12997 (6) $[C_{20}H_{30}{}^{35}Cl_2{}^{54}FeN_6]^+$, 479.13332 (1) $[C_{19}{}^{13}CH_{30}{}^{35}Cl_2{}^{54}FeN_6]^+$, 480.12529 (100) $[C_{20}H_{30}{}^{35}Cl_2FeN_6]^+$, 481.12865 (22) $[C_{19}{}^{13}CH_{30}{}^{35}Cl_2FeN_6]^+$, 482.12234 (64) $[C_{20}H_{30}{}^{35}Cl^{37}ClFeN_6]^+$, 483.12570 (14) $[C_{19}{}^{13}CH_{30}{}^{35}Cl^{37}ClFeN_6]^+$, 484.11939 (10) $[C_{20}H_{30}{}^{37}Cl_2FeN_6]^+$, 485.12275 (2) $[C_{19}{}^{13}CH_{30}{}^{37}Cl_2FeN_6]^+$, 486.12610 (<1) $[C_{18}{}^{13}C_2H_{30}{}^{37}Cl_2FeN_6]^+$; found: 478.13097 (6), 479.13409 (1), 480.12639 (100), 481.12914 (25), 482.12358 (63), 483.12621 (16), 484.12130 (11), 485.12349 (2), 486.12586 (<1). EA ($C_{20}H_{30}Cl_2FeN_6$): calculated C 49.92%; H 6.28%; N 17.46%. Found C 49.84%; H 6.16%; N 17.63%.

Additional information on the synthesis of the target compound and original analysis data files are available *via* the Chemotion repository: **https://dx.doi.org/10.14272/reaction/SA-FUHFF-UHFFFADPSC-QUQGCQVELV-UHFFFADPSC-NUHFF-LUHFF-NUHFF-ZZZ**.

$[Fe(TMG_2e)Cl_2]$ (C3). Inside a nitrogen-filled glovebox, anhydrous iron(II) chloride (63 mg, 0.50 mmol, 1.0 equiv.) was dissolved in acetonitrile (3 mL) under heating. The ligand TMG_2e (**L3**, 128 mg, 0.500 mmol, 1.00 equiv.) was dissolved in acetonitrile (5 mL) at 20 °C. The iron(II) chloride solution was passed through a filter into the ligand solution. Immediately an off-white precipitate formed. The mixture was further stirred for 30 min at 20 °C. The supernatant was removed and the precipitate was washed with diethyl ether (2 × 2 mL). The volatile compounds were removed under reduced pressure to obtain the complex $[Fe(TMG_2e)Cl_2]$ (**C3**, 111 mg, 0.290 mmol, 58% yield) as an off-white solid. Colorless single-crystals suitable for single-crystal X-ray diffraction were obtained by recrystallization from acetonitrile.

IR (ATR, $\tilde{\nu}$) = 3003 (vw), 2983 (vw, $\nu(CH_{aliph})$), 2943 (w, $\nu(CH_{aliph})$), 2893 (w, $\nu(CH_{aliph})$), 2851 (w, $\nu(CH_{aliph})$), 2822 (w, $\nu(CH_{aliph})$), 2804 (vw), 1554 (vs, $\nu(C{=}N_{gua})$), 1521 (vs, $\nu(C{=}N_{gua})$), 1476 (m), 1462 (w), 1442 (w), 1424 (s), 1415 (m), 1408 (m), 1389 (vs), 1342 (m), 1326 (w), 1240 (m), 1210 (w), 1151 (s), 1123 (w), 1109 (w), 1079 (w), 1068 (s), 1043 (s), 1017 (w), 914 (w), 894 (s), 776 (w), 765 (s), 735 (w), 595 (w), 583 (vw), 578 (w), 553 (w), 500 (w), 493 (w), 489 (vw), 438 (vw), 432 (vw) cm^{-1}. HR-MS (APCI+, MeCN), *m/z* (%): isotopic distribution calculated for $[C_{12}H_{28}Cl_2FeN_6]^+$ $[M]^+$: 380.11432 (6) $[C_{12}H_{28}{}^{35}Cl_2{}^{54}FeN_6]^+$, 382.10964 (100) $[C_{12}H_{28}{}^{35}Cl_2FeN_6]^+$, 383.11300 (13) $[C_{11}{}^{13}CH_{28}{}^{35}Cl_2FeN_6]^+$, 384.10670 (64) $[C_{12}H_{28}{}^{35}Cl^{37}ClFeN_6]^+$, 385.11005 (8) $[C_{11}{}^{13}CH_{28}{}^{35}Cl^{37}ClFeN_6]^+$, 386.10374 (10) $[C_{12}H_{28}{}^{37}Cl_2FeN_6]^+$, 387.10710 (1) $[C_{11}{}^{13}CH_{28}{}^{37}Cl_2FeN_6]^+$; found: 382.10950 (100), 384.10689 (57). EA ($C_{12}H_{28}Cl_2FeN_6$): calculated C 37.62%; H 7.37%; N 21.93%. Found C 37.53%; H 7.22%; N 22.10%.

Additional information on the synthesis of the target compound and original analysis data files are available *via* the Chemotion repository: **https://dx.doi.org/10.14272/reaction/SA-FUHFF-UHFFFADPSC-CMAKKIUQDS-UHFFFADPSC-NUHFF-LUHFF-NUHFF-ZZZ**.

$[Fe(TMG_2p)Cl_2]$ (C4). Inside a nitrogen-filled glovebox, anhydrous iron(II) chloride (63 mg, 0.50 mmol, 1.0 equiv.), the ligand TMG_2p (**L4**, 135 mg, 0.500 mmol, 1.00 equiv.) and acetonitrile (3 mL) were heated until the iron(II) chloride was fully dissolved. The hot solution was filtered and layered with diethyl ether (5 mL). Over the course of 24 h, colorless crystals of the complex $[Fe(TMG_2p)Cl_2]$ (**C4**, 80 mg, 0.20 mmol, 40% yield) formed. Single crystals suitable for single-crystal X-ray diffraction were prepared by recrystallization from acetonitrile.

IR (ATR, $\tilde{\nu}$) = 3003 (vw), 2926 (w), 2911 (w, $\nu(CH_{aliph})$), 2894 (w, $\nu(CH_{aliph})$), 2856 (w, $\nu(CH_{aliph})$), 1613 (vw), 1545 (vs, $\nu(C{=}N_{gua})$), 1532 (vs, $\nu(C{=}N_{gua})$), 1477 (vw), 1465 (vw), 1440 (vw), 1421 (m), 1404 (vw), 1393 (s), 1360 (w), 1354 (w), 1342 (w), 1236 (w), 1195 (vw), 1167 (w), 1160 (w), 1151 (w), 1145 (w), 1120 (vw), 1100 (vw), 1083 (w), 1074 (vw), 1067 (vw), 1058 (vw), 1034 (m), 939 (m), 915 (w), 901 (vw), 834 (w), 774 (s), 765 (w), 724 (vw), 715 (vw), 576 (w), 525 (vw), 506 (w) cm^{-1}. HR-MS (ESI+, MeCN), *m/z* (%): calculated for $[C_{13}H_{30}Cl_2FeN_6]^+$ $[M]^+$: 396.12529, not found; only an adduct of the ligand **L4** was found: 271.26151 (100) $[C_{13}H_{31}N_6]^+$ [**L4** + H]$^+$. EA ($C_{13}H_{30}Cl_2FeN_6$): calculated C 39.31%; H 7.61%; N 21.16%. Found C 39.29%; H 7.29%; N 21.49%.

Additional information on the synthesis of the target compound and original analysis data files are available *via* the Chemotion repository: **https://dx.doi.org/10.14272/reaction/SA-FUHFF-UHFFFADPSC-OCIRWSBUTV-UHFFFADPSC-NUHFF-LUHFF-NUHFF-ZZZ**.

$[Fe(TMGpy)_2Cl]Cl$ (C5). Inside a nitrogen-filled glovebox, anhydrous iron(II) chloride (63 mg, 0.50 mmol, 1.0 equiv.) was dissolved in acetonitrile (3 mL) under heating. This solution was passed through a filter into a solution of the ligand TMGpy (**L5**, 206 mg, 1.00 mmol, 2.00 equiv.) in acetonitrile (2 mL). The resulting red solution was stirred for 30 min at 20 °C. By vapor diffusion of diethyl ether, green crystals of the complex $[Fe(TMGpy)_2Cl]Cl$ (**C5**, 116 mg, 0.215 mmol, 43% yield) formed over the course of 3 days.

IR (ATR, $\tilde{\nu}$) = 3016 (vw, $\nu(CH_{arom})$), 2983 (vw), 2947 (vw, $\nu(CH_{aliph})$), 2890 (vw, $\nu(CH_{aliph})$), 2874 (vw, $\nu(CH_{aliph})$), 2832 (vw), 1602 (w), 1577 (w), 1570 (m), 1536 (vs, $\nu(C{=}N_{gua})$), 1477 (m), 1463 (w), 1453 (w), 1437 (m), 1427 (m), 1421 (w), 1408 (w), 1393 (vs), 1370 (m), 1291 (w), 1257 (vw), 1234 (w), 1158 (s), 1147 (w), 1111 (vw), 1096 (vw), 1069 (w), 1063 (w), 1056 (w), 1019 (w), 1012 (w), 1009 (w), 981 (vw), 914 (w), 896 (vw), 856 (vw), 846 (vw), 802 (m), 777 (vs), 744 (vw), 727 (w), 643 (w), 618 (w), 579 (w), 576 (w), 553 (vw), 486 (vw) cm^{-1}. HR-MS (APCI+, MeOH), *m/z* (%): isotopic distribution calculated for $[C_{22}H_{36}Cl_2FeN_8]^+$ $[M]^+$: 536.18306 (6) $[C_{22}H_{36}{}^{35}Cl_2{}^{54}FeN_8]^+$, 537.18642 (2) $[C_{21}{}^{13}CH_{36}{}^{35}Cl_2{}^{54}FeN_8]^+$, 538.17839 (100) $[C_{22}H_{36}{}^{35}Cl_2FeN_8]^+$, 539.18175 (24) $[C_{21}{}^{13}CH_{36}{}^{35}Cl_2FeN_8]^+$, 540.17544 (64) $[C_{22}H_{36}{}^{35}Cl^{37}ClFeN_8]^+$, 541.17880 (15) $[C_{21}{}^{13}CH_{36}{}^{35}Cl^{37}ClFeN_8]^+$, 542.17249 (10) $[C_{22}H_{36}{}^{37}Cl_2FeN_8]^+$, 543.17585 (2) $[C_{21}{}^{13}CH_{36}{}^{37}Cl_2FeN_8]^+$, 544.17920 (<1) $[C_{20}{}^{13}C_2H_{36}{}^{37}Cl_2FeN_8]^+$; found: 538.1787 (100), 539.1831 (8), 540.1761 (47). EA ($C_{22}H_{36}Cl_2FeN_8$): calculated C 48.99%; H 6.73%; N 20.78%. Found C 48.73%; H 6.66%; N 21.16%.

Additional information on the synthesis of the target compound and original analysis data files are available *via*

the Chemotion repository: **https://dx.doi.org/10.14272/reaction/SA-FUHFF-UHFFFADPSC-YBCYHBWFSB-UHFFFADPSC-NUHFF-LUHFF-NUHFF-ZZZ**.

[Fe(TMGepy)Cl_2] (C6). Inside a nitrogen-filled glovebox, anhydrous iron(II) chloride (63 mg, 0.50 mmol, 1.0 equiv.) was dissolved in acetonitrile (4 mL) under heating. The resulting solution was added to the ligand TMGepy (**L6**, 110 mg, 0.500 mmol, 1.00 equiv.). The mixture was shaken (*circa* 1 min) and filtered. By vapor diffusion of diethyl ether, the complex [Fe(TMGepy)Cl_2] (**C6**, 108 mg, 0.311 mmol, 62% yield) formed as green crystals over the course of 24 h.

IR (ATR, $\tilde{\nu}$) = 3061 (vw, $\nu(CH_{arom})$), 3010 (vw, $\nu(CH_{arom})$), 2927 (w, $\nu(CH_{aliph})$), 2900 (w, $\nu(CH_{aliph})$), 2875 (w, $\nu(CH_{aliph})$), 2845 (w), 2806 (vw), 1603 (w), 1537 (vs, $\nu(C{=}N_{gua})$), 1485 (m), 1480 (m), 1459 (w), 1452 (w), 1442 (s), 1423 (s), 1416 (w), 1405 (s), 1395 (vs), 1360 (w), 1345 (s), 1305 (w), 1258 (w), 1238 (w), 1230 (w), 1219 (w), 1161 (m), 1143 (m), 1115 (w), 1110 (w), 1073 (w), 1062 (w), 1054 (w), 1027 (w), 1017 (vw), 984 (m), 969 (w), 907 (w), 876 (w), 797 (w), 781 (vs), 765 (s), 748 (w), 716 (w), 646 (w), 590 (w), 581 (w), 511 (m), 458 (m), 417 (w) cm^{-1}. HR-MS (APCI+, MeOH), *m*/*z* (%): isotopic distribution calculated for $[C_{12}H_{20}Cl_2FeN_4]^+$ $[M]^+$: 344.04557 (6) $[C_{12}H_{20}{}^{35}Cl_2{}^{54}FeN_4]^+$, 345.04892 (<1) $[C_{11}{}^{13}CH_{20}{}^{35}Cl_2{}^{54}FeN_4]^+$, 346.04090 (100) $[C_{12}H_{20}{}^{35}Cl_2FeN_4]^+$, 347.04425 (13) $[C_{11}{}^{13}CH_{20}{}^{35}Cl_2FeN_4]^+$, 348.03795 (64) $[C_{12}H_{20}{}^{35}Cl^{37}ClFeN_4]^+$, 349.04130 (8) $[C_{11}{}^{13}CH_{20}{}^{35}Cl^{37}ClFeN_4]^+$, 350.03500 (10) $[C_{12}H_{20}{}^{37}Cl_2FeN_4]^+$, 351.03835 (1) $[C_{11}{}^{13}CH_{20}{}^{37}Cl_2FeN_4]^+$; found: 346.04117 (100), 347.04587 (23), 348.03838 (63), 349.04296 (14), 350.03576 (7). EA ($C_{12}H_{20}Cl_2FeN_4$): calculated C 41.53%; H 5.81%; N 16.14%. Found C 41.54%; H 6.05%; N 16.40%.

Additional information on the synthesis of the target compound and original analysis data files are available *via* the Chemotion repository: **https://dx.doi.org/10.14272/reaction/SA-FUHFF-UHFFFADPSC-SUGFTNYFKC-UHFFFADPSC-NUHFF-LUHFF-NUHFF-ZZZ**.

[Fe(DMEG$_2$b)Cl_2] (C7). Inside a nitrogen-filled glovebox, anhydrous iron(II) chloride (63 mg, 0.50 mmol, 1.0 equiv.) was dissolved in acetonitrile (3 mL) under heating. The resulting solution was added to the ligand DMEG$_2$b (**L7**, 150 mg, 0.500 mmol, 1.00 equiv.). The mixture was shaken until the ligand was fully dissolved and was filtered. By vapor diffusion of diethyl ether, the complex [Fe(DMEG$_2$b)Cl_2] (**C7**, 120 mg, 0.281 mmol, 56% yield) was obtained as green crystals over the course of 5 days.

IR (ATR, $\tilde{\nu}$) = 2955 (w, $\nu(CH_{aliph})$), 2928 (w, $\nu(CH_{aliph})$), 2888 (w), 2870 (w, $\nu(CH_{aliph})$), 1588 (m), 1547 (vs, $\nu(C{=}N_{gua})$), 1528 (vs, $\nu(C{=}N_{gua})$), 1479 (vs), 1461 (m), 1459 (m), 1450 (m), 1412 (vs), 1378 (vs), 1292 (s), 1281 (vs), 1235 (w), 1202 (vw), 1187 (vw), 1161 (vw), 1114 (w), 1079 (vw), 1036 (vs), 976 (m), 939 (vw), 887 (m), 856 (w), 811 (m), 761 (vs), 739 (vs), 705 (m), 663 (vw), 646 (w), 604 (w), 586 (w), 557 (m), 499 (w), 478 (w), 471 (w), 447 (vw), 428 (vw), 417 (vw) cm^{-1}. HR-MS (APCI+, MeCN/MeOH), *m*/*z* (%): isotopic distribution calculated for $[C_{16}H_{24}Cl_2FeN_6]^+$ $[M]^+$: 424.08302 (6) $[C_{16}H_{24}{}^{35}Cl_2{}^{54}FeN_6]^+$, 425.08637 (1) $[C_{15}{}^{13}CH_{24}{}^{35}Cl_2{}^{54}FeN_6]^+$, 426.07834 (100) $[C_{16}H_{24}{}^{35}Cl_2FeN_6]^+$, 427.08170 (17) $[C_{15}{}^{13}CH_{24}{}^{35}Cl_2FeN_6]^+$, 428.07539 (64) $[C_{16}H_{24}{}^{35}Cl^{37}ClFeN_6]^+$, 429.07875 (11) $[C_{15}{}^{13}CH_{24}{}^{35}Cl^{37}ClFeN_6]^+$, 430.07244 (10) $[C_{16}H_{24}{}^{37}Cl_2FeN_6]^+$, 431.07580 (2) $[C_{15}{}^{13}CH_{24}{}^{37}Cl_2FeN_6]^+$; found: 424.08303 (6), 426.07859 (100), 427.08201 (23), 428.07576 (61), 429.07910 (13), 430.07363 (10). EA ($C_{16}H_{24}Cl_2FeN_6$): calculated C 44.99%; H 5.66%; N 19.67%. Found C 44.88%; H 5.63%; N 19.81%.

Additional information on the synthesis of the target compound and original analysis data files are available *via* the Chemotion repository: **https://dx.doi.org/10.14272/reaction/SA-FUHFF-UHFFFADPSC-LGNUUDHCCJ-UHFFFADPSC-NUHFF-LUHFF-NUHFF-ZZZ**.

[Fe(DMEG$_2$n)Cl_2] (C8). Inside a nitrogen-filled glovebox, anhydrous iron(II) chloride (63 mg, 0.50 mmol, 1.0 equiv.) was dissolved in acetonitrile (3 mL) under heating. The ligand DMEG$_2$n (**L8**, 175 mg, 0.500 mmol, 1.00 equiv.) was dissolved in acetonitrile (3 mL) at 20 °C. The iron(II) chloride solution was passed through a filter into the ligand solution. Immediately, an orange precipitate formed. The mixture was shaken (*circa* 1 min). After settling, the supernatant was removed. The solid was washed with diethyl ether (3 × 2 mL) and after removing the volatile compounds under reduced pressure, the complex [Fe(DMEG$_2$n)Cl_2] (**C8**, 209 mg, 0.438 mmol, 88% yield) was obtained as an orange solid. Single crystals suitable for single-crystal X-ray diffraction were obtained by recrystallization from acetonitrile.

IR (ATR, $\tilde{\nu}$) = 2951 (vw, $\nu(CH_{aliph})$), 2890 (w, $\nu(CH_{aliph})$), 2868 (w, $\nu(CH_{aliph})$), 2797 (vw, $\nu(CH_{aliph})$), 1583 (w), 1544 (vs, $\nu(C{=}N_{gua})$), 1505 (w), 1489 (w), 1477 (m), 1463 (w), 1448 (w), 1427 (w), 1408 (s), 1387 (w), 1373 (w), 1342 (w), 1322 (w), 1294 (vs), 1239 (w), 1209 (w), 1164 (w), 1139 (w), 1127 (w), 1089 (w), 1060 (w), 1025 (m), 1009 (s), 977 (m), 969 (m), 921 (vw), 893 (vw), 852 (m), 823 (w), 810 (m), 783 (s), 770 (vs), 703 (w), 651 (w), 635 (m), 603 (w), 595 (w), 533 (m), 500 (s), 472 (m), 451 (vw), 435 (w), 431 (w), 423 (w), 414 (w) cm^{-1}. HR-MS (ESI+, MeCN), *m*/*z* (%): isotopic distribution calculated for $[C_{20}H_{26}Cl_2FeN_6]^+$ $[M]^+$: 474.0987 (6) $[C_{20}H_{26}{}^{35}Cl_2{}^{54}FeN_6]^+$, 475.1020 (1) $[C_{19}{}^{13}CH_{26}{}^{35}Cl_2{}^{54}FeN_6]^+$, 476.0940 (100) $[C_{20}H_{26}{}^{35}Cl_2FeN_6]^+$, 477.0973 (22) $[C_{19}{}^{13}CH_{26}{}^{35}Cl_2FeN_6]^+$, 478.0910 (64) $[C_{20}H_{26}{}^{35}Cl_{37}ClFeN_6]^+$, 479.0944 (14) $[C_{19}{}^{13}CH_{26}{}^{35}Cl^{37}ClFeN_6]^+$, 480.0881 (10) $[C_{20}H_{26}{}^{37}Cl_2FeN_6]^+$, 481.0914 (2) $[C_{19}{}^{13}CH_{26}{}^{37}Cl_2FeN_6]^+$; found: 474.0975 (2), 476.0936 (100), 477.0964 (21), 478.0912 (68), 479.0933 (13), 480.0890 (9). EA ($C_{20}H_{26}Cl_2FeN_6$): calculated C 50.34%; H 5.49%; N 17.61%. Found C 49.98%; H 5.21%; N 17.90%.

Additional information on the synthesis of the target compound and original analysis data files are available *via* the Chemotion repository: **https://dx.doi.org/10.14272/reaction/SA-FUHFF-UHFFFADPSC-CHWOIVIIAO-UHFFFADPSC-NUHFF-LUHFF-NUHFF-ZZZ**.

Bulk polymerization of L-lactide

Inside a nitrogen-filled glovebox, the catalyst, L-lactide (LLA) and, if appropriate, the co-initiator *p*-methyl benzyl alcohol (*p*MeBnOH), $FeCl_2$ or the ligand TMG$_2$e (**L3**) were

homogenized in a mortar for 10 min. The mixture was transferred to a vial and removed from the glovebox. The used steel reactor was pre-heated under vacuum to the desired reaction temperature and flooded with argon gas for three times over the course of 1 h. The polymerization mixture was transferred to the reactor under a counter stream of argon. As soon as the reactor was closed, the mechanical stirrer was started and the acquisition of Raman spectra was initiated. After the desired reaction time, the stirrer and heating were turned off and the reactor was opened. An NMR sample for the determination of the conversion was taken. The residual polymer melt was distributed to two vials. The first fraction was used as a retention sample and the second fraction was dissolved in DCM (3–5 mL depending on the viscosity), precipitated from EtOH at 20 °C and the volatile compounds were removed under reduced pressure. The precipitated polymer was subjected to GPC analysis in order to determine the molar mass and the molar mass distribution.

Methanolysis of polylactide

For the depolymerization experiments, PLA (0.25 g, amount of ester linkages n_{EL} = 3.5 mmol, 1.0 eq.), the catalyst (0.035 mmol, 1 mol%), and absolute THF (4.0 mL) were added to a Young-type Schlenk tube inside a nitrogen-filled glovebox. The PLA and the catalyst were dissolved using an external heat source and placed in an oil bath at 60 °C. The reaction was started by addition of dry MeOH (1.00 mL, 24.7 mmol, 7.13 eq., THF/MeOH = 4 : 1) and stirred at 260 rpm. Samples were analyzed by ^{1}H NMR spectroscopy in $CDCl_3$.

Data availability

Additional information on the synthesis and characterization of the presented iron(II) guanidine complexes is available *via* the Chemotion repository. The respective links are given in the Experimental section.

Crystallographic data for complexes **C1–C8** has been deposited at the Cambridge Crystallographic Data Centre (CCDC) as supplementary no. CCDC – 2278549 for **C1**, CCDC – 2278550 for **C2**, CCDC – 2278551 for **C3**, CCDC – 2278552 for **C4**, CCDC – 2278553 for **C5**, CCDC – 2278554 for **C6**, CCDC – 2278555 for **C7** and CCDC – 2278556 for **C8**.

Original data of polymerization and depolymerization experiments as well as the MALDI-TOF-MS spectra are available *via* the RADAR4Chem repository by FIZ Karlsruhe – Leibniz-Institut für Informationsinfrastruktur and are published under an Open Access model (CC BY-NC-SA 4.0 Attribution-NonCommercial-Share Alike: DOI: **https://doi.org/10.22000/1625**).

Author contributions

CC: conceptualization; methodology, investigation, formal analysis and data curation for complex synthesis & characterization and polymerization experiments; visualization, writing – original draft. LB: methodology, investigation, formal analysis and data curation for depolymerization experiments; writing – review & editing. SS: investigation (complex synthesis & characterization, polymerization experiments), writing – review & editing. SN: investigation (complex synthesis & characterization, polymerization experiments), writing – review & editing. YK: investigation (depolymerization experiments), writing – review & editing. JH: investigation, formal analysis (conducted DFT calculations); writing – review & editing. AH: supervision, validation, data curation, writing – review & editing. SHP: conceptualization, supervision, funding acquisition, resources, writing – review & editing.

Conflicts of interest

There are no conflicts to declare.

Acknowledgements

We thank the European Commission under Horizon 2020 Grant Agreement no. 953073 (UPLIFT project) for funding. Moreover, we would like to thank bio-mi Ltd. (Matulji, Croatia) for the supply with PLA and TotalEnergies Corbion (Gorinchem, Netherlands) for the donation of lactide. We thank the RWTH High Performance Computing Cluster for computing time. We acknowledge Christian Broschinski, Maverick Eilers and Kristofer Weinberg for experimental support. We thank Henrika Hüppe for performing single-crystal X-ray diffraction measurements. We are grateful to Brigitte Pütz for conducting mass spectrometry and Brigitte Jansen for conducting TGA measurements (both IAC, RWTH Aachen University). In addition, we would like to thank Prof. Dr. Andrij Pich and Marion Connolly (both DWI – Leibniz-Institut für Interaktive Materialien, Aachen) for the MALDI-TOF-MS measurements. Finally, we thank NFDI4Chem for support and funding of the repositories Chemotion repository and RADAR4Chem.

References

1 R. E. Drumright, P. R. Gruber and D. E. Henton, *Adv. Mater.*, 2000, **12**, 1841–1846.
2 R. A. Auras, L.-T. Lim, S. E. M. Selke and H. Tsuji, *Poly(Lactic Acid): Synthesis, Structures, Properties, Processing, Applications, and End of Life*, Wiley, Hoboken, NJ, USA, 2nd edn, 2022.
3 R. Auras, B. Harte and S. Selke, *Macromol. Biosci.*, 2004, **4**, 835–864.
4 P. McKeown and M. D. Jones, *Sustainable Chem.*, 2020, **1**, 1–22.
5 J. Payne, P. McKeown and M. D. Jones, *Polym. Degrad. Stab.*, 2019, **165**, 170–181.
6 H. R. Kricheldorf and I. Kreiser-Saunders, *Makromol. Chem.*, 1990, **191**, 1057–1066.
7 M. Baśko and P. Kubisa, *J. Polym. Sci., Part A: Polym. Chem.*, 2006, **44**, 7071–7081.

8 N. E. Kamber, W. Jeong, R. M. Waymouth, R. C. Pratt, B. G. G. Lohmeijer and J. L. Hedrick, *Chem. Rev.*, 2007, **107**, 5813–5840.
9 O. Dechy-Cabaret, B. Martin-Vaca and D. Bourissou, *Chem. Rev.*, 2004, **104**, 6147–6176.
10 T. Rosen, J. Rajpurohit, S. Lipstman, V. Venditto and M. Kol, *Chem. – Eur. J.*, 2020, **26**, 17183–17189.
11 J. Payne, P. McKeown, G. Kociok-Köhn and M. D. Jones, *Chem. Commun.*, 2020, **56**, 7163–7166.
12 P. Marin, M. J.-L. Tschan, F. Isnard, C. Robert, P. Haquette, X. Trivelli, L.-M. Chamoreau, V. Guérineau, I. del Rosal, L. Maron, V. Venditto and C. M. Thomas, *Angew. Chem., Int. Ed.*, 2019, **58**, 12585–12589.
13 B. B. Idage, S. B. Idage, A. S. Kasegaonkar and R. V. Jadhav, *Mater. Sci. Eng., B*, 2010, **168**, 193–198.
14 K. R. Delle Chiaie, A. B. Biernesser, M. A. Ortuño, B. Dereli, D. A. Iovan, M. J. T. Wilding, B. Li, C. J. Cramer and J. A. Byers, *Dalton Trans.*, 2017, **46**, 12971–12980.
15 S. Impemba, F. Della Monica, A. Grassi, C. Capacchione and S. Milione, *ChemSusChem*, 2020, **13**, 141–145.
16 B. J. O'Keefe, L. E. Breyfogle, M. A. Hillmyer and W. B. Tolman, *J. Am. Chem. Soc.*, 2002, **124**, 4384–4393.
17 J. A. Stewart, P. McKeown, O. J. Driscoll, M. F. Mahon, B. D. Ward and M. D. Jones, *Macromolecules*, 2019, **52**, 5977–5984.
18 P. V. S. Nylund, B. Monney, C. Weder and M. Albrecht, *Catal. Sci. Technol.*, 2022, **12**, 996–1004.
19 A. Thevenon, C. Romain, M. S. Bennington, A. J. P. White, H. J. Davidson, S. Brooker and C. K. Williams, *Angew. Chem., Int. Ed.*, 2016, **55**, 8680–8685.
20 P. McKeown, L. A. Román-Ramírez, S. Bates, J. Wood and M. D. Jones, *ChemSusChem*, 2019, **12**, 5233–5238.
21 J. Stewart, M. Fuchs, J. Payne, O. Driscoll, G. Kociok-Köhn, B. D. Ward, S. Herres-Pawlis and M. D. Jones, *RSC Adv.*, 2022, **12**, 1416–1424.
22 A. Buchard, C. J. Chuck, M. G. Davidson, G. Gobius du Sart, M. D. Jones, S. N. McCormick and A. D. Russell, *ACS Catal.*, 2023, **13**, 2681–2695.
23 C. Hermans, W. Rong, T. P. Spaniol and J. Okuda, *Dalton Trans.*, 2016, **45**, 8127–8133.
24 M. Save, M. Schappacher and A. Soum, *Macromol. Chem. Phys.*, 2002, **203**, 889–899.
25 Z. Zhong, P. J. Dijkstra and J. Feijen, *Angew. Chem., Int. Ed.*, 2002, **41**, 4510–4513.
26 S. Jacobsen, H. G. Fritz, P. Degée, P. Dubois and R. Jérôme, *Polym. Eng. Sci.*, 1999, **39**, 1311–1319.
27 P. M. Schäfer and S. Herres-Pawlis, *ChemPlusChem*, 2020, **85**, 1044–1052.
28 A. Hermann, T. Becker, M. A. Schäfer, A. Hoffmann and S. Herres-Pawlis, *ChemSusChem*, 2022, **15**, e202201075.
29 A. Hermann, S. Hill, A. Metz, J. Heck, A. Hoffmann, L. Hartmann and S. Herres-Pawlis, *Angew. Chem., Int. Ed.*, 2020, **59**, 21778–21784.
30 M. Fuchs, P. M. Schäfer, W. Wagner, I. Krumm, M. Walbeck, R. Dietrich, A. Hoffmann and S. Herres-Pawlis, *ChemSusChem*, 2023, **16**, e202300192.
31 S. Herres-Pawlis, A. Neuba, O. Seewald, T. Seshadri, H. Egold, U. Flörke and G. Henkel, *Eur. J. Org. Chem.*, 2005, **2005**, 4879–4890.
32 J. Stanek, T. Rösener, A. Metz, J. Mannsperger, A. Hoffmann and S. Herres-Pawlis, *Guanidines as Reagents and Catalysts II*, 2015, pp. 95–164, DOI: **10.1007/7081_2015_173**.
33 S. Pohl, M. Harmjanz, J. Schneider, W. Saak and G. Henkel, *J. Chem. Soc., Dalton Trans.*, 2000, 3473–3479, DOI: **10.1039/B002554M**.
34 S. Pohl, M. Harmjanz, J. Schneider, W. Saak and G. Henkel, *Inorg. Chim. Acta*, 2000, **311**, 106–112.
35 H. Wittmann, A. Schorm and J. Sundermeyer, *Z. Anorg. Allg. Chem.*, 2000, **626**, 1583–1590.
36 J. Börner, S. Herres-Pawlis, U. Flörke and K. Huber, *Eur. J. Inorg. Chem.*, 2007, **2007**, 5645–5651.
37 J. Börner, U. Flörke, K. Huber, A. Döring, D. Kuckling and S. Herres-Pawlis, *Chem. – Eur. J.*, 2009, **15**, 2362–2376.
38 P. M. Schäfer, M. Fuchs, A. Ohligschläger, R. Rittinghaus, P. McKeown, E. Akin, M. Schmidt, A. Hoffmann, M. A. Liauw, M. D. Jones and S. Herres-Pawlis, *ChemSusChem*, 2017, **10**, 3547–3556.
39 P. M. Schäfer, P. McKeown, M. Fuchs, R. D. Rittinghaus, A. Hermann, J. Henkel, S. Seidel, C. Roitzheim, A. N. Ksiazkiewicz, A. Hoffmann, A. Pich, M. D. Jones and S. Herres-Pawlis, *Dalton Trans.*, 2019, **48**, 6071–6082.
40 R. D. Rittinghaus, P. M. Schäfer, P. Albrecht, C. Conrads, A. Hoffmann, A. N. Ksiazkiewicz, O. Bienemann, A. Pich and S. Herres-Pawlis, *ChemSusChem*, 2019, **12**, 2161–2165.
41 R. D. Rittinghaus, A. Karabulut, A. Hoffmann and S. Herres-Pawlis, *Angew. Chem., Int. Ed.*, 2021, **60**, 21795–21800.
42 R. D. Rittinghaus, J. Zenner, A. Pich, M. Kol and S. Herres-Pawlis, *Angew. Chem., Int. Ed.*, 2022, **61**, e202112853.
43 M. Fuchs, M. Walbeck, E. Jagla, A. Hoffmann and S. Herres-Pawlis, *ChemPlusChem*, 2022, **87**, e202200029.
44 L. Burkart, A. Eith, A. Hoffmann and S. Herres-Pawlis, *Chem. – Asian J.*, 2023, **18**, e202201195.
45 M. Kawahata, K. Yamaguchi, T. Ito and T. Ishikawa, *Acta Crystallogr., Sect. E: Struct. Rep. Online*, 2006, **62**, o3301–o3302.
46 V. Raab, J. Kipke, R. M. Gschwind and J. Sundermeyer, *Chem. – Eur. J.*, 2002, **8**, 1682–1693.
47 M. Kawahata, K. Yamaguchi and T. Ishikawa, *Cryst. Growth Des.*, 2005, **5**, 373–377.
48 V. Raab, K. Harms, J. Sundermeyer, B. Kovačević and Z. B. Maksić, *J. Org. Chem.*, 2003, **68**, 8790–8797.
49 A. Hoffmann, J. Börner, U. Flörke and S. Herres-Pawlis, *Inorg. Chim. Acta*, 2009, **362**, 1185–1193.
50 R. Wortmann, A. Hoffmann, R. Haase, U. Flörke and S. Herres-Pawlis, *Z. Anorg. Allg. Chem.*, 2009, **635**, 64–69.
51 L. Yang, D. R. Powell and R. P. Houser, *Dalton Trans.*, 2007, 955–964, DOI: **10.1039/B617136B**.
52 A. W. Addison, T. N. Rao, J. Reedijk, J. van Rijn and G. C. Verschoor, *J. Chem. Soc., Dalton Trans.*, 1984, 1349–1356, DOI: **10.1039/DT9840001349**.
53 N. Conen, M. Fuchs, A. Hoffmann, S. Herres-Pawlis and A. Jupke, *Adv. Sustainable Syst.*, 2023, **7**, 2200359.

54 M. Reinmuth, U. Wild, D. Rudolf, E. Kaifer, M. Enders, H. Wadepohl and H.-J. Himmel, *Eur. J. Inorg. Chem.*, 2009, **2009**, 4795–4808.
55 I. d. S. Vieira, *PhD Thesis*, Technische Universität Dortmund, 2013.
56 J. Börner, *PhD Thesis*, Universität Paderborn, 2009.
57 P. Roquette, A. Maronna, M. Reinmuth, E. Kaifer, M. Enders and H.-J. Himmel, *Inorg. Chem.*, 2011, **50**, 1942–1955.
58 V. N. Staroverov, G. E. Scuseria, J. Tao and J. P. Perdew, *J. Chem. Phys.*, 2003, **119**, 12129–12137.
59 J. Tao, J. P. Perdew, V. N. Staroverov and G. E. Scuseria, *Phys. Rev. Lett.*, 2003, **91**, 146401.
60 A. Schäfer, C. Huber and R. Ahlrichs, *J. Chem. Phys.*, 1994, **100**, 5829–5835.
61 K. Eichkorn, F. Weigend, O. Treutler and R. Ahlrichs, *Theor. Chem. Acc.*, 1997, **97**, 119–124.
62 F. Weigend and R. Ahlrichs, *Phys. Chem. Chem. Phys.*, 2005, **7**, 3297–3305.
63 S. Grimme, S. Ehrlich and L. Goerigk, *J. Comput. Chem.*, 2011, **32**, 1456–1465.
64 L. Goerigk and S. Grimme, *Phys. Chem. Chem. Phys.*, 2011, **13**, 6670–6688.
65 A. Hoffmann, R. Grunzke and S. Herres-Pawlis, *J. Comput. Chem.*, 2014, **35**, 1943–1950.
66 E. D. Glendening, C. R. Landis and F. Weinhold, *J. Comput. Chem.*, 2019, **40**, 2234–2241.
67 E. D. Glendening, J. K. Badenhoop, A. E. Reed, J. E. Carpenter, J. A. Bohmann, C. M. Morales, P. Karafiloglou, C. R. Landis and F. Weinhold, *NBO (7.0)*, Theoretical Chemistry Institute, University of Wisconsin, Madison, WI, USA, 2018.
68 L. A. Román-Ramírez, P. McKeown, M. D. Jones and J. Wood, *ACS Catal.*, 2019, **9**, 409–416.
69 W. L. F. Armarego, *Purification of laboratory chemicals, Part 1: Physical techniques, chemical techniques, organic chemicals*, Butterworth-Heinemann, Amsterdam, Netherlands, 9th edn, 2022.